On Efficient Collision Schemes in the Direct Simulation Monte Carlo (DSMC): From micro/nano flows to hypersonic flows

Ehsan Roohi, Stefan K Stefanov

On Efficient Collision Schemes in the Direct Simulation Monte Carlo (DSMC): From micro/nano flows to hypersonic flows

Ehsan Roohi [*], Stefan Stefanov

High Performance Computing (HPC) Laboratory, Department of Mechanical Engineering, Ferdowsi University of Mashhad, 91775-1111, Mashhad, Iran

Institute of Mechanics, Bulgarian Academy of Science, Acad. G. Bontchev str., 1113, Sofia, Bulgaria

Abstract

The motivation of this review paper is to present a detailed summary of different collision models developed in the framework of the direct simulation Monte Carlo (DSMC) method. The emphasis is put on a newly developed collision model, i.e., the Simplified Bernoulli trial (SBT), which permits efficient low-memory simulation of rarefied gas flows. The paper starts with a brief review of the governing equations of the rarefied gas dynamics including Boltzmann and Kac master equations and reiterates that the linear Kac equation reduces to a non-linear Boltzmann equation under the assumption of molecular chaos. An introduction to the DSMC method is provided, and principles of collision algorithms in the DSMC are discussed. A distinction is made between those collision models that are based on classical kinetic theory (time counter, no time counter (NTC), and nearest neighbor (NN)) and the other class that could be derived mathematically from the Kac master equation (pseudo-Poisson process, ballot box, majorant frequency, Null collision, Bernoulli trial and its variants). To provide a deeper insight, the

[*] Author to whom correspondence should be addressed, Associate Prof., Tel: +98 (51) 38805136, Fax: +98 (051) 38763304, Email: e.roohi@ferdowsi.um.ac.ir

derivation of both collision models, either from the principles of the kinetic theory or the Kac master equation, is provided with sufficient details. Some discussions on the importance of subcells in the DSMC collision procedure are also provided and different types of subcells are presented. The paper then focuses on the simplified version of the Bernoulli trials algorithm (SBT) and presents a detailed summary of validation of the SBT family collision schemes (SBT on transient adaptive subcells: SBT-TAS, and intelligent SBT: ISBT) for a broad spectrum of rarefied gas-flow test cases, ranging from low speed, internal nano flows to external hypersonic flow, emphasizing first the accuracy of these new collision models and second, demonstrating that the SBT family scheme, if compared to other conventional and recent collision models, requires small number of particles per cell to obtain sufficiently accurate solutions.

Keywords: Rarefied flow, Boltzmann equation, Kac master equations, DSMC, collision models, simplified Bernoulli trials, micro/nano flows, hypersonic flow.

Contents

1. Introduction

With the rapid progress in design and utilization of micro/nano-electro-mechanical-system (MEMS/NEMS), the requirement for detailed analysis of fluid and thermal characteristics in these systems increases. Flow in MEMS/NEMS reveals rarefied behavior as the characteristic length of these devices is comparable to the gas mean free path. Therefore, flow treatment in MEMS/NEMS requires the same numerical approach as the flow over high altitude flying objects. The scaling parameter determining the degree of flow rarefaction is the Knudsen number,

which is defined as the ratio of the gas mean free path (λ) to the characteristics dimension (L) of the geometry. That is Kn= λ/L. Different rarefaction regimes are defined according to the Knudsen number, i.e., continuum (Kn<0.001), slip (0.001<Kn<0.1), transition (0.1<Kn<10), and free molecular (Kn>10) [1]. However, it should be reminded that this classification is mainly based on data obtained from experiments and numerical studies of isothermal gaseous flows in long one-dimensional (1D) microchannels. For flows in 2D and 3D complex geometries, the range of above regimes is debatable and should be reconsidered for each studied problem separately [2]. The fundamental kinetic equations describing the rarefied gas flow are the Boltzmann nonlinear equation [3] and its probabilistic alternative the linear Kac stochastic equation [4-5].

Direct simulation Monte Carlo (DSMC) is a statistical approach widely employed for treating rarefied gas flows [6-8]. The straightforwardness and strong physical logic of its procedures are some of the advantages of the DSMC method for studying rarefied gas flows. The basic DSMC is defined as a numerical particle representation of the Boltzmann equation. However, Kac stochastic equation was also utilized to derive alternative collision models [9-10]. The first published paper on DSMC by Graeme Bird was concerned to the simulation of a 0-D relaxation problem [11]. In that paper, 30,000 collision events per hour were simulated using the hard sphere model of 500 simulator particles. With today's computers, more than 10 billion collision events can be simulated per hour for this relaxation problem. Progress in computer technology and development of new DSMC models has allowed for very complex physics to be modeled in the DSMC method, i.e., chemical reactions, evaporation, and condensation of substances, ionization and radiation [12-13]. In DSMC, the time evolution of the particle system within a small time interval (Δt) is split into two consecutive steps – free motion of all particles and collisions of particles localized in the neighborhoods of given points in the space, i.e. in cells of a computational grid assuming fixed their coordinates and changing only their velocities in results

of binary collisions. The collision algorithm plays the significant role in the DSMC method and calculates the most sophisticated term of the Boltzmann or Kac stochastic equation. In this review we are focused on the more complicated collision step, which defines the basic features of the DSMC method. The DSMC schemes could be categorized into two general classes/groups concerning the treatment of collisions. Considering the Boltzmann definition for the kinetic equation of a rarefied gas, the concept of the first -group of collision schemes is based on the principle of the maximum collision rate per time step. In this group, the "No Time Counter (NTC)" [14] scheme, considers a superior number of maximum collision rate per time step which determines the number of randomly selected particle pairs that should be checked for accepted collision, while the other methods in this group, e.g. "Time Counter (TC)" [15], "Null Collision (NC)" [16-17], and "Majorant Frequency Scheme (MFS)" [10] use a time-interval of δt_i for each captured collision and a time-step interval of Δt for the DSMC procedure, and continue the collision process until $\sum_i \delta t_i > \Delta t$. It should be noted that besides the inherent discretization problems of deterministic numerical approaches, DSMC calculations are accompanied by two extra problems: (a) the presence of statistical noise in output results, and (b) the dependence of results on the number of particles per cell and possibility of repeated collisions. It has been shown [18-21] that a modified variance reduced Monte Carlo simulation, which takes into account the asymptotic properties of near continuum low-speed regimes, is capable of overcoming the first problem. In response to the second problem, other type collision schemes, proposed by Belotserkovskii and Yanitskiy [22] and Yanitskiy [9], were constructed on the base of the Kac stochastic equation. Contrary to the former group of collision schemes, the latter group, in accordance with the Kac stochastic model, defines a collision probability function for each particle pair and check all pair combinations for collision occurrence. The Yanitskiy approach [9, 22] then led to the introduction of the Bernoulli-Trials collision scheme (BT) which benefitted from the avoidance of the repeat collisions. Stefanov introduced a simplified variant of the Bernoulli Trials scheme entitled as 'SBT' [23-24]. Unlike the former scheme (BT), which has a

quadratic dependency of the computational cost on the particle number in cells, the latter one (SBT) has a linear dependency and a higher computational efficiency. As an evolution of the SBT scheme to a method which can intelligently prefer collisions for closer pairs, Goshayeshi et al. [25] introduced an intelligent variant of the SBT scheme entitled as "ISBT" which provides semi-cognition of distance for the collision scheme. This semi-cognition reduces approximately 25-32% of the overall mean collision separation distance (MCS) in collision cells. Understanding the recent notes of Gallis et al. [26-27] in the preference of choosing a near neighbor partner rather than the nearest neighbor one, which consequently leads to the saving of the collision scheme from losing some of its probable collisions during the advection phase of particles, the ISBT scheme also follows the same strategy of near neighbor pair-selection.

Considering the fact that smaller mean collision separation distances would cause more realistic collisions and prevent from the angular momentum reduction, the modifications have been proposed to both groups of collision schemes. Based on the logic of the first group, LeBeau et al. [28] introduced the virtual sub-cell (VSC) method which performs an $O(N^2)$ operation to sort all N simulators in a cell to find the nearest-neighbor to any simulator chosen for collision. Alternatively, Bird [29] proposed the transient adaptive sub-cell (TAS) scheme that subdivides cells into sub-cells, and collision pairs are selected from the same or neighboring sub-cells. In the second group of collision schemes, however, there were some constraints in the development of modifications to reduce MCS. For instance, because the collision process is conducted in a hierarchical order of indexed particles, it is not possible to directly search for the nearest pair in such a way like the VSC does, or search in the neighboring subcells in a way that NTC-TAS does. Therefore, in the case of TAS usage, it became only possible to have subcells adapted with 4-5 particles. Therefore, the selection of the nearest-neighbor in the second group of collision schemes is bound with the nearer neighbor selection [30].

The aim of the current review is to present and evaluate a recent Kac-based collision model in the direct simulation Monte Carlo (DSMC) method, Simplified Bernoulli trial (SBT) and its variants,

i.e., SBT on transient adaptive subcells (SBT-TAS) and intelligent SBT (ISBT) in the treatment of a wide spectrum of rarefied gas flows either at micro/nano scales or hypersonic flow regimes. Accuracy, memory and CPU requirements, time consumption and rigorousness of this collision family will be discussed in details. The paper continues with a derivation of the mathematical relation between the Boltzmann and Kac master equations and then introduces the collision schemes based on classical kinetic theory (Boltzmann Equation) in the DSMC method followed by the derivation of Kac-based family collision models such as the Bernoulli trial (BT) and Simplified Bernoulli trial family schemes and presentation of validations of the SBT collision family.

2. Collision models based on the Boltzmann equation

The most detailed level of description of a system consisting of large number (N) of molecules is given by the Newton equation. The evolution equations of this system are given by [31]:

$$m_j \frac{d^2 \vec{x}_j}{dt^2} = \sum_{i \neq j}^{N} R_{ij} \tag{1}$$

, where R_{ij} is the force between pair (i-j). However, the solution of such a system is difficult due to requirement of specifying of the initial coordinates and velocity of each molecule in the system, complexity of the force function, as well as solving a $3N$ differential-coupled equation. Following the Gibbs formalism, rather than considering a single system, an ensemble of systems in the $6N$-dimensional (3 space and 3 velocity coordinate, i.e. phase space, for each particle) is distributed according to the N-particle velocity (probability) distribution function (F_N). This ensemble system could be treated by the Liouville equation, which describes the time evolution of the phase space distribution function [31]:

$$\frac{\partial F_N}{\partial t} + \sum_{i=1}^{N} c_i \frac{\partial F_N}{\partial x_i} + \sum_{i \neq j}^{N} \sum_{i=1}^{N} \frac{R_{ij}}{m} \frac{\partial F_N}{\partial c_i} = 0 \tag{2}$$

The Liouville equation and all the succeeding kinetic equations following from the BBGKY hierarchy (Bogoliubov–Born–Green–Kirkwood–Yvon hierarchy, or sometimes called Bogoliubov hierarchy) including the last Boltzmann equation have a probabilistic nature because their main unknown is the probability distribution function. Though Liouville equation is simpler than the Newton equation, it considers collisions of N molecules and its solution is quite challenging. A less expensive description is attained by approximating the flow description using only n-particle distribution functions, which determine the probability to simultaneously find n particles independently of the state of the remaining (N–n) particles. Following the BBGKY hierarchy, a chain of linked equations could be obtained for reduced n-particle distribution functions, where the equation for the single-particle distribution function $f(t, x^{(l)}, c)$ corresponds to the Boltzmann equation, which considers only binary collisions. The flowchart of hierarchy of the governing equations is shown in Fig. 1. Boltzmann equation does not describe the motion of particles, as Newton's equation does, but the time-dependent change of the probability distribution function. In fact, the Boltzmann equation is a nonlinear, seven-dimensional, integro-differential equation governing the spatio-temporal evolution equation of the one-particle velocity distribution function $f(t, x^{(l)}, c)$. The velocity distribution function quantifies the number of particles, $f(t, x^{(l)}, c)\, \mathrm{d}x^{(l)}\, \mathrm{dc}$, which are located in an infinitesimal volume $dx^{(l)}$ at position $x^{(l)}$ and whose velocities are in the infinitesimal interval dc around c. The Boltzmann equation is given by [32]

$$\frac{\partial}{\partial t}(nf) + c.\frac{\partial}{\partial r}(nf) + F.\frac{\partial}{\partial c}(nf) = \int_{-\infty}^{\infty}\int_{0}^{4\pi} n^2\left(f^* f_1^* - f f_1\right) c_r\, \sigma\, d\Omega\, dc_1 \qquad (3)$$

, where n is number density, t is time, r is space vector, c is velocity space vector, F is external force per unit mass, c_r is the relative velocity between a molecule of velocity class c and one with velocity class c_1, $\sigma_T\, \mathrm{d}\Omega$ is the differential cross-section for the collision of a molecule of class c with another one having class c_1 such that their post-collision velocities are c^* and c_1^*,

respectively, and functions f, f_1, f^* and f_1^* are the corresponding velocity distribution functions for the molecule and its collision partner before and after the collisions. In fact, f is the probability of finding a particle in the velocity space volume element d^3c around c, provided that the particle is located in the space volume element d^3x around x. Collision in the Boltzmann equation is an instantaneous, random jump process in particles velocity localized in a point. Boltzmann equation is valid for dilute gasses so that only binary collisions between the molecules are possible. The sophisticated and nonlinear properties of the collision integral and its containing of seven variables create severe difficulties for the numerical analysis of the Boltzmann equation. High dimensionality and probabilistic nature of the kinetic processes as well as complex molecular collision models are among the main prerequisites for the application of the direct simulation Monte Carlo method to handle the Boltzmann equation. Direct simulation Monte Carlo, as developed by Bird [6], is a numerical simulation of the evolution of a collection of particles. Historically, the application of Monte Carlo method for rarefied gas flows was initiated by the pioneering works of Kogan and Perepukhov for simulation of free-molecular flows around flying objects [32]. In fact, Bird used principles of Monte Carlo method, such as acceptance-rejection, to perform numerical computations of the collision terms of the Boltzmann equation, as will be described in the following section. It should be noted that the first DSMC application by Bird was aimed for simple homogeneous relaxation problems, in which a non-equilibrium gas velocity distribution is driven toward equilibrium by intermolecular collisions [11]. A flowchart depicting different collision models employed in the DSMC method is shown in Fig. 2. In the following, details of these collision models are provided with sufficient discussions.

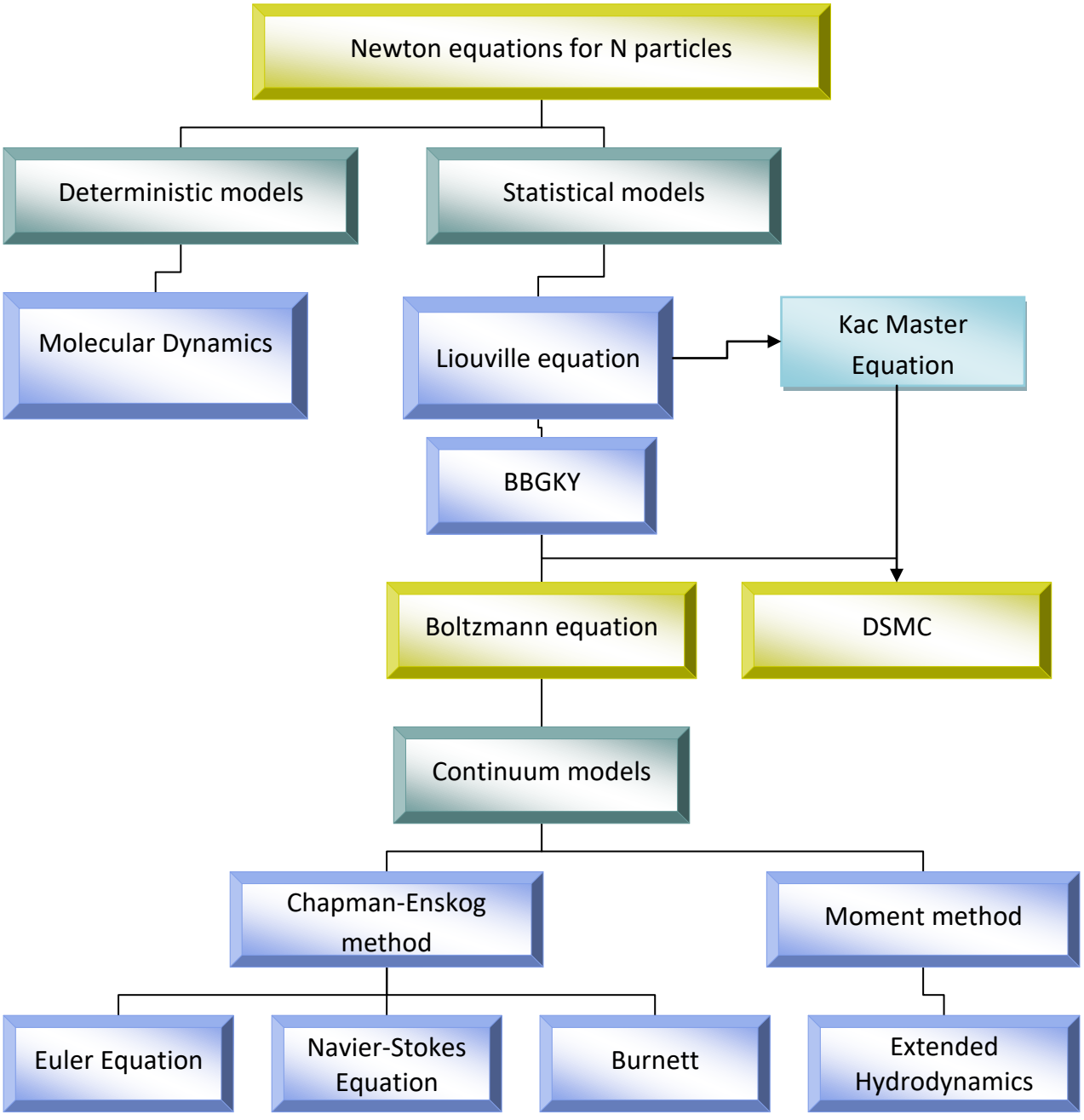

Fig. 1: Flowchart of hierarchy of governing equations

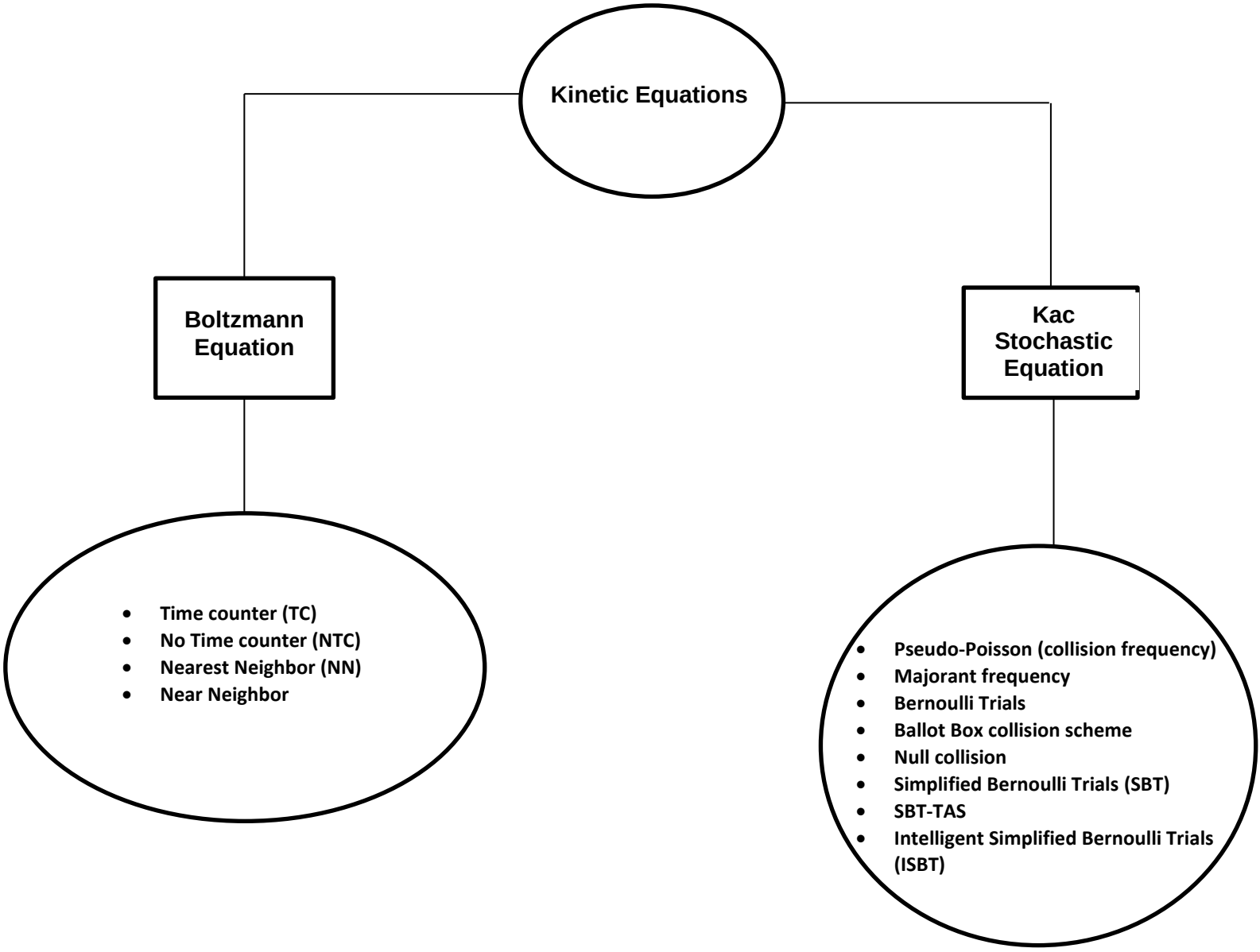

Fig. 2: DSMC collision models derived from the Boltzmann equation and Kac master equation.

2.1 Time counter (TC) collision model

The time counter method is the first collision schemes introduced by Bird [14]. In this method, the total number of collisions in a cell is assumed to be:

$$N_{Coll} = \frac{\Delta t N n F_{num} \overline{\sigma_T c_r}}{2} \tag{4}$$

Where overbar quantity means averaged valued, and $n = N/V_c$ is number density. For every particle pair chosen at random, the following time increment is added to the time counter of the cell:

$$\Delta t_{coll} = \frac{2}{NnF_{num}\,\sigma_T c_r} \tag{5}$$

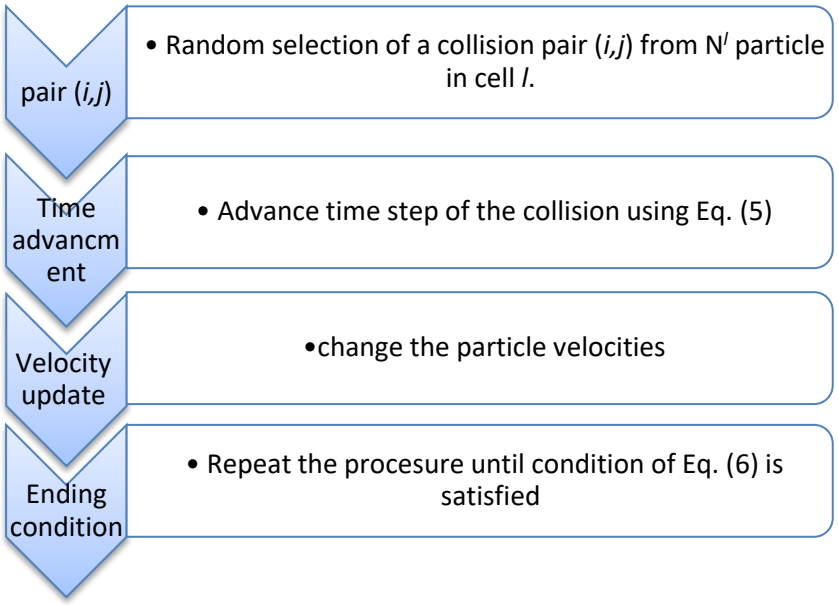

Fig. 3 TC collision procedure

The TC model assumes that each collision contributes equally in the temporal advancement of the collision numbers in the cell. The procedure is repeated until

$$\sum \Delta t_{coll} \leq \Delta t_{cell} \tag{6}$$

Flowchart of the TC collision model is shown in Fig. 3. The computational cost of TC algorithm is of the order O(*N*). It is mentioned that TC model needs around 20 particles per cell to produce correct results. However, the TC model could not produce correct solution under extreme non-equilibrium conditions such as the front of a very strong shock. In fact, the acceptance of an unlikely collision can advance the time by an interval that is much larger than the time step and

the overall collision rate can be distorted. Lutisan [33] showed that TC model could not reproduce Poisson distribution function for probability distribution of number of collisions.

2.2 No-Time-Counter (NTC) collision model [8, 14]

According to the classical kinetic theory utilized in deriving the Boltzmann equation, the collision probability (P) between two particles over the time interval dt is equal to the ratio of volume swept by their total collision cross section moving at the relative speed (c_r) to the volume of the cell which contains particles (V_c), i.e.,

$$P = F_N \sigma_T c_r dt / V_c \tag{7}$$

The average number of simulated particles in a cell is $N=nV_c/F_n$, where n is the gas number density and F_N is the ratio of number of real molecules to simulated particles. All possible collisions could be checked by choosing all N(N-1)/2 collision pairs in the cell and checking the collision probability P for all of them, i.e., collision is accepted if $P>R_{nf}$. This collision algorithm is called Bernoulli trials (BT) [9], and is inefficient because P is a small quantity and number of choices is proportional to the square of number of particles, O (N^2). To increase the efficiency of the collision procedure and reduce the computational costs to O(N), Bird suggested to repair the TC scheme by using the idea of maximum collision cross-section approach well known in Monte Carlo methods used for simulation of linear integral equations describing the transport of neutrons. The idea appears almost around the same time in the papers of Koura [16] and Bird [14]. Then, the acceptance-rejection technique and no time counter method or null-collision methods were used for the first time in DSMC. The universal acceptance-rejection technique [34] requires a superior estimation of the collision probability. It can be written as:

$$P_{max} = F_N (\sigma_T c_r)_{max} dt / V_c \tag{8}$$

The number of pair selections per time step is calculated by multiplying this equation by N(N-1)/2. Therefore, in this procedure, that is called “No Time Counter (NTC) method, the maximum number of particle pairs checked for collision is computed as:

$$N_{coll} = 1/2N(N-1)F_N(\sigma_T c_r)_{max} dt/V_c \tag{9}$$

, and this number of pairs is selected at each cell per time step, and the collision of pair (i,j) is accepted with the following probability given by Eq. (10).

$$\frac{(\sigma_T c_r)_{ij}}{(\sigma_T c_r)_{max}} > R_f \tag{10}$$

Note that initially, $(\sigma_T c_r)_{max}$ is set to an appropriately chosen reference value in each cell, and then it is updated if the product of $(\sigma_T c_r)$ of the chosen pair becomes larger than the reference value. This procedure keeps the computational expanse of NTC as O(*N)*. The sequence of NTC collision procedure is shown in Fig. 4. First, an upper limit, i.e., N_{coll} pairs to be checked is calculated; second, by using acceptance-rejection procedure the actual number of *accepted collisions* in a cell is defined.

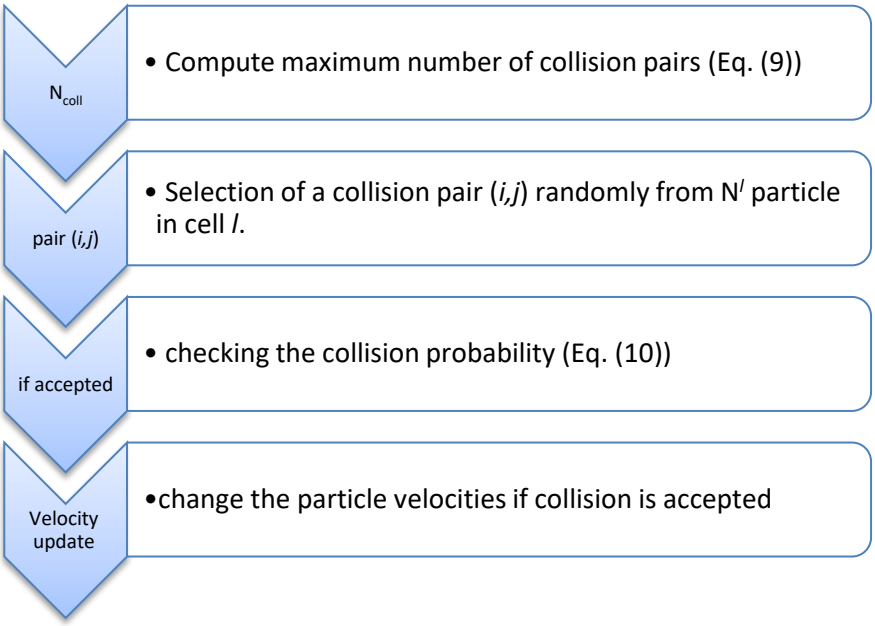

Fig. 4 NTC collision procedure, repeated N_{coll} time for each DSMC collision cell.

It should be reminded that in Bird's monograph [8], and other references describing NTC, instead the term $N(N-1)$ was written the product $N\bar{N}$, where over bar quantity means averaged value. The relation of the collision process to the Poisson distribution and its consequence, i.e., equality

of $\overline{N(N-1)} = \overline{N^2}$, were pointed out by Yanitskiy [9], then reemphasized and utilized, as given in Eq.(10), by Stefanov and Cercignani [35], and finally utilized by Bird in his sophisticated algorithm [36-37].

An insufficient number of particles per cell can be a source of stochastic errors in the NTC model. However, if enough number of particles in cells is employed, NTC scheme is an efficient approach for modeling the intermolecular collisions. But, NTC scheme is CPU demanding in complex, 3D simulations where a huge number of cells and particles are required for proper flow simulation. In fact, NTC scheme requires enough number of particles per cell, i.e., N=10-20, to provide accurate results. However, due to random selection of collision pairs, one of the main shortcomings of the NTC collision is the possibility of repeated collisions, i.e., the same pair of particles is selected repeatedly for collision within one or several successive time steps without occurrence of events of collisions with other particles. This results in inaccuracy of the collision process in cells containing small number of particles. One remedy is to construct an array and keeping track of the record of collision pairs to avoid repeated collisions for a particle pair. However, this introduces additional complexities. To use the acceptance-rejection procedure, the pairs should be chosen randomly from the whole available set of *N* particles to keep a correct probability for collision corresponding to the Boltzmann collision frequency. In this case, all probabilities and collision frequencies are calculated correctly. Direct avoiding of repeated collisions means that one introduces a condition that leads to a non-uniform distribution of probabilities, because for the first chosen pair one chooses randomly among N(N-1)/2 pair of particles but the second choice is performed from among (N)(N-1)/2-1 pairs of particles. The effect is stronger if one keeps this direct collision control condition for successive time steps. Evidently, this error is minor for large number of particles but it is of considerable importance if there are a few particles per cell. There is another disadvantage in the NTC scheme, the use of remainders to keep an accurate number of collisions in time. The problem arises from the practical calculation of N_{coll} by using eq. (9), which, in general case, is not an integer value and

the integer part of N_{coll} is used. When the number N_{coll} is large it works fine but when $N_{coll} \sim 1$ or less the reminder procedure introduces additional error related to the fact the probability distribution of the remainders gives different from the Poisson law variation of the number of collisions.

2.3 Nearest Neighbor (NN) scheme

LeBeau et al. [28] introduced the "virtual subcell" (VSC) method as an improvement in the particle selection procedure of the NTC, in which the first particle is chosen randomly, while the second partner is selected from available neighbors of the selected particle, i.e., the nearest neighbor (NN) of a given particle is found and selected. The flowchart of NN collision model is shown in Fig. 5. Method VSC needs the collision separation distance to be calculated for all available particles in the cell to find the nearest neighbor one. To reduce computational costs to O(N), Bird proposed to avoid the calculation of all intermolecular distances at the start of collision procedure and restrict to the calculation of an intermolecular distance between the first randomly chosen particle, *i*, and the nearest among the other particles.

The NTC-NN algorithm was implemented in the new versions of DSMC codes distributed by Gream Bird [13]. Bird et al. [38] and Gallis et al. [39] compared the convergence behavior of the NN collision model compared with the standard NTC one, and showed that NN achieves high efficiency as it minimizes the mean collision separation between collision partners; however, the new algorithm is very sensitive to the selection of the time step and almost for all cell needs smaller time steps compared to the original NTC. They showed that NN significantly reduces the computational resources required for a DSMC simulation to achieve a particular level of accuracy if its computational set-up is chosen appropriately. As a modification of NN model, Macrossan [40] suggested the 'pseudo-subcell' collision method, in which the search for a collision partner discontinues if a 'near-enough' particle is found, i.e. whenever another particle is found within

the ‘pseudo-subcell’ of radius δ centered on the first particle. Macrossan showed that in structured cells, the pseudo-subcell method gives a 5% increase in mean collision separation (MCS) compared to the NN method, and is up to 20% faster than the NN method.

As mentioned, NN needs lower time steps as it ignores a key point in pair selection: within a time step particles with higher velocities may reach and collide particles, which are further than their nearest neighbor; therefore, a small enough time step should be utilized. On the other hand, according to the Boltzmann equation, the working space is phase space with three coordinates (positions) and three velocities variables. From this view point, NN takes into account only the space of coordinates using the criterion of minimum distance for colliding pairs. This means that NN works well when the whole velocity distribution function is available at every coordinate point. To have this fulfilled, one should have enough particles in all small volumes. Otherwise, there will be negative effects and erroneous solutions. Bird [37] showed that NN needs at least 7 particles per collision cell to predict equilibrium collision frequency correctly.

It should be noted that Bird states that lower values of separation of free paths (SOF), which is the ratio of mean collision separation (MCS) to the mean free path (SOF=MCS/λ) largely self-validates the accuracy of DSMC solutions [13]. However, it should be mentioned that this is a necessary but not a sufficient condition. So, it should be noted that low SOF did not always guarantee correct solution if it is not accompanied with enough particle per cells (PPC) and fine enough cell.

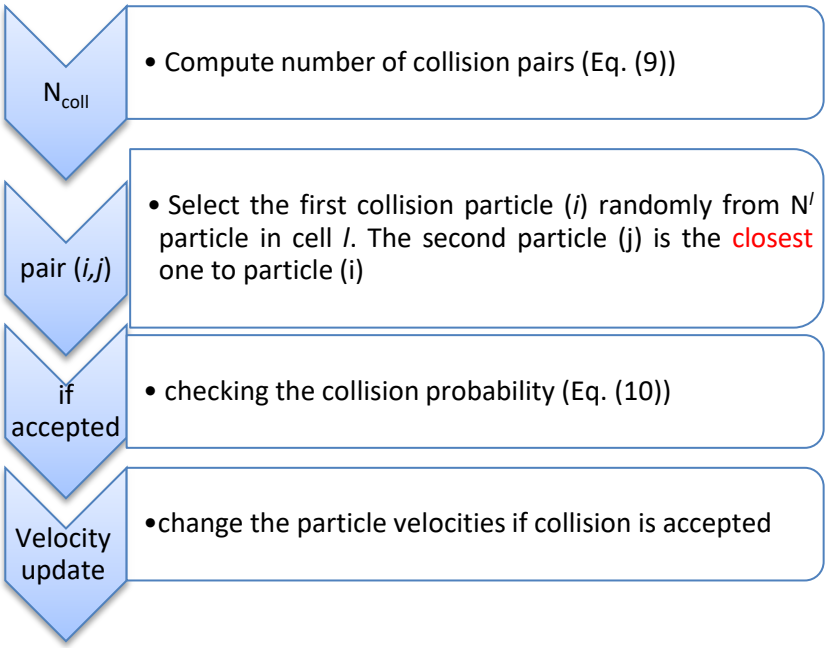

Fig. 5 NN collision procedure

2.4 A note on DSMC cells and subcells

The DSMC method uses the cell for the selection of collision partners and for the sampling of the macroscopic properties. To avoid statistical scatters and reduce inherent errors in the standard NTC method, the number of DSMC particles per cell should be as large as possible, generally around twenty. On the other hand, in the selection of collision pairs, it is desirable to choose close particles and reduce the mean collision separation of pairs and minimize the smearing of gradients. These conflicting requirements can be remedied by dividing the sampling cell into a set of sub-cells and perform pair selection and collision from inside the subcells [8]. However, the first use of the subcells was suggested after the objection raised by Meiburg [41]. As angular momentum is not conserved in a simulated collision, Meiburg [41] concluded that if colliding particles are selected from opposite sides of a cell, the collision introduces significant error. Meiburg pointed out this process in a flow with vorticity and noted that the angular velocity of the collision partners about the center of the collision is not necessarily conserved. However, Bird

mentioned that this is essentially a cell size effect, i.e., the cell size must be very small in comparison with the mean free path in regions with large gradients, such as Knudsen layers. As Bird mentioned, the problem with Meiburg's calculation was that the cells he had used had a linear dimension of 3λ which was excessively large by a factor of at least ten [42]. However, to overcome this problem, Bird [43] introduced subcells within each cell, where a potential collision partner is selected from the same subcell or from a nearby subcell if no collision partner could be found in the same subcell. Thus, the use of subcells reduces the mean collision separation (MCS) to a fraction of the subcell size, rather than a fraction of the cell size. Stefanov et al. [44-45] suggested the idea of dynamic subdivision of subcells, or as called: collision cells. They adjusted the subcell such that the subcell size remains smaller than the mean free path (λ) at every time step. In order to provide a sufficient number of subcells that is compatible with the instantaneous number of particles inside each collision cell, Bird proposed the transient adaptive subcell (TAS) technique [46-47]. TAS technique was successfully employed in combination with NTC collision model in structured [46] and unstructured cells [48].

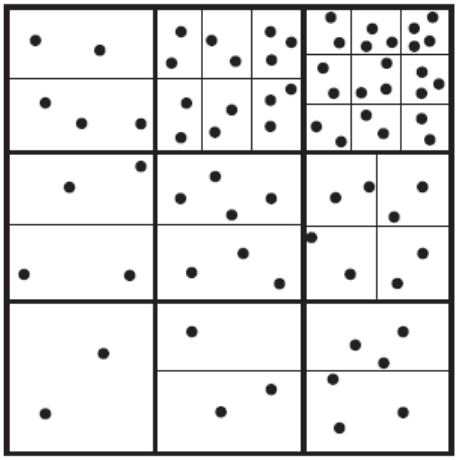

Fig. 6: Schematic of the number of subcells in each cell using TAS, bold lines depict cell borders and narrow lines depict subcell borders [49].

In fact, before reaching the steady state, the number of particles in each cell varies during the computational process; consequently, the number of transient subcells varies according to local density gradients, see Fig. 6. To determine the number of subcells in each direction in a 2-D cell, number of particles per subcell, PPSC, should be set as one of the inputs. For each cell, this transient layer of subcells is fabricated by a special number of divisions along x (D_x) and y (D_y) directions as follows:

$$D_x = \sqrt{\frac{N_c}{AR \times Envelop \times PPSC}} \tag{11}$$

$$D_y = D_x \times AR\ ;\ AR = \frac{\Delta y_{cell}}{\Delta x_{cell}};\ Envelop = \frac{V_c}{\Delta y_{cell} \times \Delta x_{cell}} \tag{12}$$

, where AR is the aspect ratio, $PPSC$ is the desired number of particles per subcell and $Envelop$ is used to increase the number of subcells, in case the cell is not fully rectangular. Using TAS, the selection of collision pairs is performed in subcells level, therefore, the effect of cell-size on the accuracy of the solution is reduced and much coarser basic collision cells could be employed. However, to apply correctly the TAS strategy one should complete it with a second element concerning the time step. The time step should be coupled with the smallest subcell size in order to fulfil the well-known Courant condition, which for the DSMC method could be replaced with a simple rule required on the stage of particle free motion i.e. the time step to be chosen small enough in order the probability for all particles to pass further than one neighboring subcell to tend to zero. As shown in section 3.9.2 this point was taken into account for controlling the time step.

In the sophisticated version of DSMC, the idea of using cells and subcells was upgraded to use separate sampling and collision cells. In the NN collision model, collision cells should be adapted to 7 particles and sampling cells are adapted to around 20 particles, respectively [37].

3. Kac Master Equation

3.1 Introduction

In the homogenous case, i.e. a kinetic equation without streaming term, the time evolution of velocity distribution function of N particle system $F_{N^{(l)}}\left(t, x^{(l)}, c_{N^{(l)}}\right)$ due to inter-molecular collision could be described by the Kac stochastic model [4-5, 9]. The Kac master equation is a probabilistic analog of Liouville equation considering only binary collisions of the particles with given probability. Consider a system of $\{x^{(l)}, C_{N^{(l)}}\} = \{x_j^{(l)}(t_k),\ c_j^{(l)}(t_k)\}, j = 1, \ldots, N^{(l)}$ particles in a cell (l) with volume $V^{(l)}$. The Kac stochastic model can be described by the following direct Kolmogorov equation:

$$\frac{\partial}{\partial t} F_{N^{(l)}}\left(t, x^{(l)}, c_{N^{(l)}}\right) = \frac{1}{V^l} \sum_{1 \le i < j \le N^l} g_{ij} \int_{4\pi} \left[F_{N^{(l)}}\left(t, x^{(l)}, {c_{N^{(l)}}}^{ij}\right) - F_{N^{(l)}}\left(t, x^{(l)}, c_{N^{(l)}}\right)\right] d\sigma_{ij} \tag{13}$$

, where $F_{N^{(l)}}\left(t, x^{(l)}, {c_{N^{(l)}}}^{ij}\right)$ is the N-particle probabilistic velocity distribution function after the collision of i-j particles, i.e., ${c_{N^{(l)}}}^{ij} = \{c_1, \ldots\ldots, c_{i-1}, c_i', c_{i-1}, \ldots\ldots, c_{j-1}, c_j', c_{j+1}, \ldots\ldots, c_{N^{(l)}}\}$, which denotes that velocities of pair *i-j* particles are updated to their post-collision velocities. The sum over $1 \le i < j \le N^l$ means summation over N(N−1)/2 collision pairs. Kac stochastic model is a linear integro-differential equation that describes the time behavior of the N-particle distribution function. In fact, The Kac stochastic model is a jump-like strictly Markovian process over the hypersphere $\Omega(N, E, P)$ of 3N-4 dimensions in Euclidean space R_{3N}, where N is the number of particles, E is the kinetic energy and P is the momentum of velocity components. This hypersphere is formed by crossing of a hypersphere of total kinetic energy of particles $c_1^2 + \cdots . + c_n^2 = E = \text{Cte}$ with three hyperplanes $c_1 + \cdots . + c_n = P = \text{Cte}$. Strictly Markovian processes are described by a pair of adjoined equations, i.e., direct and reverse Kolmogorov equations [50].

The one particle distribution function could be obtained from $F_{N^{(l)}}\left(t, x^{(l)}, {c_{N^{(l)}}}^{ij}\right)$ as follows:

$$f_1{}^{(n)}\left(c_{1,}x^{(l)},t\right)=\int_{c_2^2+\cdots+c_n^2=n-c^2}F_{N^{(l)}}\left(t,x^{(l)},c_{N^{(l)}}\right)d\sigma \tag{14}$$

, i.e., the integration over all velocity classes, expect to that of $c_{1,}$ results in a reduced distribution function of velocity class c_1. Assuming number of particles approaches infinity and using the local assumption of molecular chaos, which permits to write two-particle distribution function in terms of one particle distribution function:

$$f_2\left(c_1,c_2,x^{(l)},t\right)=f_1(c_1,x^{(l)},t)f_1(c_2,x^{(l)},t) \tag{15}$$

, the Boltzmann equation without the streaming term could be recovered from the Kac stochastic model.

In general, the hypothesis of molecular chaos is one of the most discussed assumptions in kinetic theory and statistical physics. There are not well-defined criteria for its validity. However, it can be accepted as a good approximation that the molecular chaos hypothesis is valid if the gas is close to a local equilibrium state and the provided number of particles, *N*, becomes very large. It is obvious that the Kac master equation does not require the fulfillment of molecular chaos hypothesis although it is partly used for generating stochastic collision parameters. One can conclude that all collision schemes derived from the Kac master equation keep this property. Following this line, it could be shown that most of collision schemes, except the Nanbu collision scheme [17], have a more direct connection to the Kac master equation than the Boltzmann equation. In fact, similar to Liouville equation, Kac model contains all possible correlation between particles velocities. Reducing N-particle distribution function via BBGKY chain of equations one consequently neglects (N-1)-particle correlation functions. The last is all binary correlation functions, among them are self-correlations functions that means velocity and other kind of fluctuations. The last relation between velocity distribution functions is between two-particle and one-particle distribution functions, which reads as:

$$f_2\left(c_1,c_2,x^{(l)},t\right)=f_1\left(c_1,x^{(l)},t\right)f_1\left(c_2,x^{(l)},t\right)+Corr(c_1,c_2) \tag{16}$$

Where $Corr(c_1, c_2)$ corresponds to correlations between distribution functions of c_1 and c_2. Molecular chaos assumption means $Corr(c_1, c_2) = 0$, which leads to equality (15) employed in the derivation of the Boltzmann equation. Thus, the correlations do not exist in the Boltzmann equation solution. But DSMC can evaluate them realistically as shown in the Bird's monograph [8] and supported, for example, by numerical results shown in Ref. [44] obtained for velocity correlations and fluctuations showing that the DSMC method adequately evaluates binary correlation functions, which cannot be obtained from the Boltzmann equation. This circumstance determines the place of the DSMC method in flowchart of hierarchy of the governing equation shown in Fig. 1. However, it should be noted that the calculation of the maximum collision rate used in collision schemes based on TC and NTC collision algorithms is founded on the Eq. (4) of the classic Boltzmann kinetic theory, which reflects on the classification of the models given in Fig. 2.

In the operator form, Kac stochastic model, Eq. (13), could be written as follows [9]:

$$\frac{\partial}{\partial t} F_{N^{(l)}}\left(t, x^{(l)}, c_{N^{(l)}}\right) = \left[\sum_{1 \le i < j \le N^l} w_{ij}\left(T_{ij} - I\right)\right] F_{N^{(l)}}\left(t, x^{(l)}, c_{N^{(l)}}\right) = \upsilon(T - I) F_{N^{(l)}}\left(t, x^{(l)}, c_{N^{(l)}}\right) \tag{17}$$

, where

$$I\psi = \psi, \quad T_{ij} = \int_{4\pi} \psi\left(c_{ij}\right) B\left(g_{ij}, \theta\right) d\Omega(\theta), \tag{18}$$

$$T\psi = \sum_{1 \le i < j \le N^l} w_{ij}\, T_{ij}\psi \tag{19}$$

, and $B\left(g_{ij}, \theta\right)$ is a scattering kernel [51]. The transformation $T_{ij} F_{N^{(l)}}\left(t, x^{(l)}, c_{N^{(l)}}\right)$ results in probability density distribution of ${c_{N^{(l)}}}^{ij}$ over $\Omega(N, E, P)$ after the collision of a pair (c_i, c_j) under the condition that before the collision point $c_{N^{(l)}}$ is distributed over $\Omega(N, E, P)$ with the probability density $F_{N^{(l)}}\left(t, x^{(l)}, c_{N^{(l)}}\right)$.

In the Kac model, the probability of time interval between two successive collisions is distributed according to the exponential distribution of a Poisson process as follows:

$$Prob(\delta t > t) = e^{-\upsilon t}$$

$$\upsilon = \sum_{1 \le i < j \le N^l} w_{ij}\,; \qquad w_{ij} = \frac{\sigma_{ij} g_{ij}}{V^l} \tag{20}$$

, where collision probability of pair (i, j) as denoted by (w_{ij}) is a function of σ_{ij}, which is the collision cross-section, and $g_{ij} = |c_i - c_j|$, which is the particles relative velocities.

In case of the given state at time t_0, the operator form of the Kac master equation could be solved at time t with the definition of the transition operator $G(t)$ in the following form:

$$F_{N^{(l)}}\left(t, x^{(l)}, C_{N^{(l)}}\right) = G(t)\, F_{N^{(l)}}(t_0, x^{(l)}, C_{N^{(l)}}) \tag{21}$$

Where the transition operator $G(t)$ could be written as:

$$G(t) = exp\left[t \sum_{1 \le i < j \le N^l} w_{ij}\left(T_{ij} - I\right)\right] = \exp[tv(T - I)] \tag{22}$$

In the next sections, following Yanitskiy [9], a family of collision models derived from Kac stochastic model and built from different variations of the exponential transitional operator formula, Eq. (22), will be discussed. These collision models define a collision probability function for each particle pair and checks all pair combinations for collision. In fact, the modeling of collision is converted to a statistical realization of the evolution of Kac's model during a period of time.

3.2 A Pseudo-Poisson Process (Collision Frequency Technique)

Considering small time step, we could assume: $\upsilon = \upsilon_c + O(t)$, neglecting the higher order terms, the operator G is approximated as follows [9]:

$$G_1(t) = exp\left[t\upsilon_c\left(T_{ij} - I\right)\right] = \exp(-t\upsilon_c)\sum_{s=0}^{\infty}\frac{(t\upsilon_c)^s}{s!}T^s \tag{23}$$

$$\text{where: } T = \sum_{1\le i<j\le N^l} W_{ij}\,T_{ij}; \qquad W_{ij} = \frac{w_{ij}}{\upsilon_c} \tag{24}$$

The above-mentioned algorithm is exact for pseudo-Maxwellian molecules, where the collision probability does not depends on relative velocity, and it has an order of accuracy of O(t) in the general case. Frequency υ_c is computed at each time step and order of computations is O (N^2). Sampling of the number of collisions $s(t)$ is performed according to probability distribution $P(t\upsilon_c)$. A pair of colliding particles is sampled with the probability of W_{ij}.

For non-Maxwellian gases, the following algorithm is performed [52] (see Fig. 7):

1- Collision time for a pair of (i, j) with velocities (V, V_1) is sampled form the exponential distribution with the collision frequency υ_c as follows:

$$Prob(\delta t_c) = \upsilon_c e^{-\upsilon_c t} \tag{25}$$

In an inverse sampling method widely employed in the Monte Carlo method, the sampled time step is given by:

$$\delta t_c = \frac{-ln(R_{nf})}{\upsilon_c} \tag{26}$$

The above procedure is continued until $\sum \delta t_c$ exceeds cell time step. The pseudo-Poisson process was applied for the first time by Koura in the collision model [52] for counting the collision of a non-Maxwellian gas, where the collision frequency was computed as follows:

$$\upsilon_c \approx \frac{F_N}{V_c}\sum_{i=1}^{N}\sum_{j=1,\neq i}(\sigma_{ij}g_{ij}) \tag{27}$$

However, in this case one needs to choose a pair for collision with a given probability. For this purpose, Koura derived it from the Boltzmann assumption of molecular chaos (for details see

[52]). This fact led us to link the Koura's approach more to the Boltzmann equation, than the Kac stochastic model.

It should be reminded that σ_{ij} is a function of relative velocity and other gas properties, i.e. for variable had sphere gases, it is given by:

$$\sigma_{ij} = \pi d_{ref}^2 \frac{1}{\Gamma(2.5-\omega)} \left(\frac{2kT_{ref}}{m_r g^2}\right)^{\omega-0.5} \tag{28}$$

Where ω is the viscosity-temperature exponent: it is equal to 0.5 for hard sphere gases and is equal to 1 for Maxwell molecules [8]. Main drawbacks of the collision frequency technique are the significant time required for computation of Eq. (27) and the assumption of constant υ_c during the time step; which requires the condition of $\Delta\upsilon_c/\upsilon_c \ll 1$, where $\Delta\upsilon_c$ is the difference between υ_c at two successive time steps.

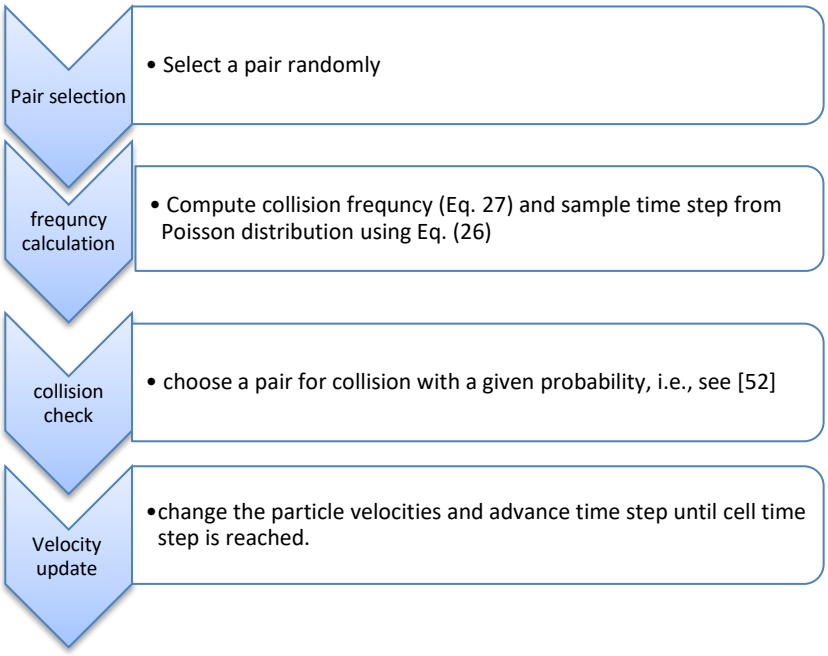

Fig. 7 Pseudo-Poisson (collision frequency) collision procedure.

3.3 Majorant frequency scheme (MFS) collision scheme

Majorant frequency scheme (MFS) could be derived either from the Leontovich master kinetic equation (MKE), which describes the behavior of an N-particle gas model with binary collisions [10, 53-54], or from the Kac master equation [55]. Similar to Kac master equation, Leontovich equation may be transformed to the Boltzmann equation as $N\rightarrow\infty$ and the molecular chaos condition is satisfied. Full details of the derivation of the MFS scheme from the Kac master equation is provided in Ref. [55]. In the MFS scheme, the time between two eventual collisions is computed from a Poisson distribution with the maximum (majorant) probability value as follows:

$$Prob(\delta t_c) = \upsilon_{max} e^{-\upsilon_{max} t} \tag{29}$$

$$\delta t_c = \frac{-ln(R_{nf})}{\upsilon_{max}} \tag{30}$$

The collisional pair is uniformly chosen from $N(N-1)/2$ available pairs. The majorant frequency is defined as:

$$\upsilon_{max} = 1/2N(N-1)F_N(\sigma_T c_r)_{max}/V_c \tag{31}$$

MFS scheme starts with calculating this frequency. MFS performs as many collisions in one time step until the summation of computed δt_c's exceeds the specified cell time step. The procedure of MFS collision is shown in Fig. 8. More details of MFS scheme and its validation could be found in Refs. [10, 55]. It is worth noting that the choice of the collision frequency in form Eq. (31), which contains an assumption for statistical independency of molecular velocities, and respectively, is based on the molecular chaos hypothesis, is important for understanding the stochastic properties of the MFS collision algorithm and its close relation with the Bird's NTC scheme. The MFS model improves the probabilistic characteristics of the process by including the Poisson process for determining the maximum number of pairs of particles. Unlike Bird's NTC, in MFS it is an integer random number obeying the Poisson law and its averaged value within a time step is exactly equal to the calculated in NTC maximum number of particle pairs to check

for collision by using Eq. (9). Thus, the MFS algorithm avoids the use of reminders, included in NTC to balance the integer number of collisions during the simulation.

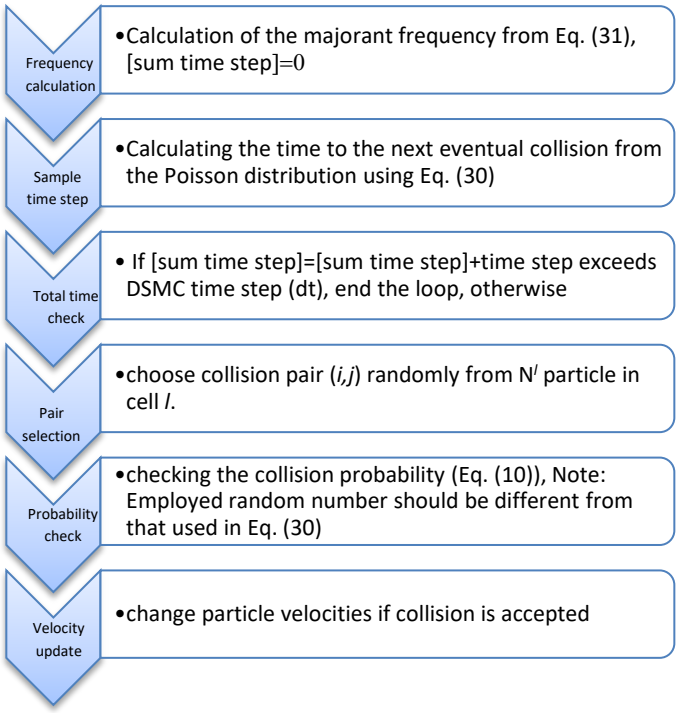

Fig. 8 The Majorant Frequency Scheme procedure per each cell.

3.4 Bernoulli Trials [9]

For small interval t, operator G(t) can be expanded with respect to t degrees and terms of order equal or higher than $O(t^2)$ are neglected. The transition operator G(t) corresponding to this approximation is obtained as:

$$G_2(t) \approx \prod_{1 \le i < j \le N^l} exp\left[t\left(T_{ij} - I\right)w_{ij}\right] = \prod_{i=1}^{N-1} \prod_{j=i+1}^{N} \exp\left[t\left(T_{ij} - I\right)w_{ij}\right] \tag{32}$$

One could replace the exponential term in every co-factor in Eq. (32) by a linear approximation over t, thus:

$$G_2(\mathrm{t}) = \prod_{\mathrm{i}=1}^{\mathrm{N}^{(\mathrm{l})}-1} \prod_{\mathrm{j}=\mathrm{i}+1}^{\mathrm{N}^{(\mathrm{l})}} \left[\left(1 - tw_{ij}\right)\mathrm{I} + tw_{ij}\mathrm{T}_{\mathrm{ij}}\right] = \prod_{\mathrm{i}=1}^{\mathrm{N}^{(\mathrm{l})}-1} \prod_{\mathrm{j}=\mathrm{i}+1}^{\mathrm{N}^{(\mathrm{l})}} \left[\left(1 - \mathrm{W}_{\mathrm{ij}}\right)\mathrm{I} + \mathrm{W}_{\mathrm{ij}}\mathrm{T}_{\mathrm{ij}}\right] \tag{33}$$

, where

$$\mathrm{W}_{\mathrm{ij}} = \frac{\sigma_{ij} g_{ij} t}{V^{(l)}}. \tag{34}$$

Every co-factor in the right-hand-side of Eq. (33) transforms the probability distribution function $F_{N^{(l)}}\left(t, x^{(l)}, c_{N^{(l)}}\right)$ over $\Omega(N, E, P)$ into $\overline{F_{N^{(l)}}}\left(t, x^{(l)}, c_{N^{(l)}}\right)$ over $\Omega(N, E, P)$ according to:

$$\overline{F_{N^{(l)}}}\left(t, x^{(l)}, c_{N^{(l)}}\right) = \left(1 - \mathrm{tw}_{\mathrm{ij}}\right) F_{N^{(l)}}\left(t, x^{(l)}, c_{N^{(l)}}\right) + \mathrm{tw}_{\mathrm{ij}} \int_{4\pi} \psi\left(c_{ij}\right) B\left(g_{ij}, \theta\right) d\Omega(\theta) \tag{35}$$

If the time step *t* is considered small such that:

$$p_{ij} = tw_{ij} \leq 1 \tag{36}$$

For all possible values of $c_{N^{(l)}}$, Eq. (33) may have an apparent probability approach. The collision scheme based on Eq. (33) considers all N(N-1)/2 pairs of particles (c_i, c_j) and to consider the collision of each pair of (c_i, c_j) with probability p_{ij}. This scheme is of first order accuracy in terms of time but its computational costs is of order N^2. The condition given by Eq. (36) could be replaced with a weaker one as follows:

$$P\{tw_{ij} > 1\} \ll 1 \tag{37}$$

by choosing appropriate time step and cell size. The above procedure states that for all of the available particle pairs in the collision cell (*l*), the acceptance-rejection should be checked, i.e. the following inequality should be checked for all available particle pairs(i,j) $\{\mathrm{i} < \mathrm{j} = 1, \ldots, \mathrm{N}^{(\mathrm{l})}\}$ (before their velocities are changed to post collision values):

$$\mathrm{W}_{\mathrm{ij}} = \frac{\sigma_{\mathrm{ij}} \mathrm{g}_{\mathrm{ij}} \mathrm{t}}{\mathrm{V}^{(\mathrm{l})}} > R_{nf} \tag{38}$$

The procedure of SBT is depicted in Fig. 9.

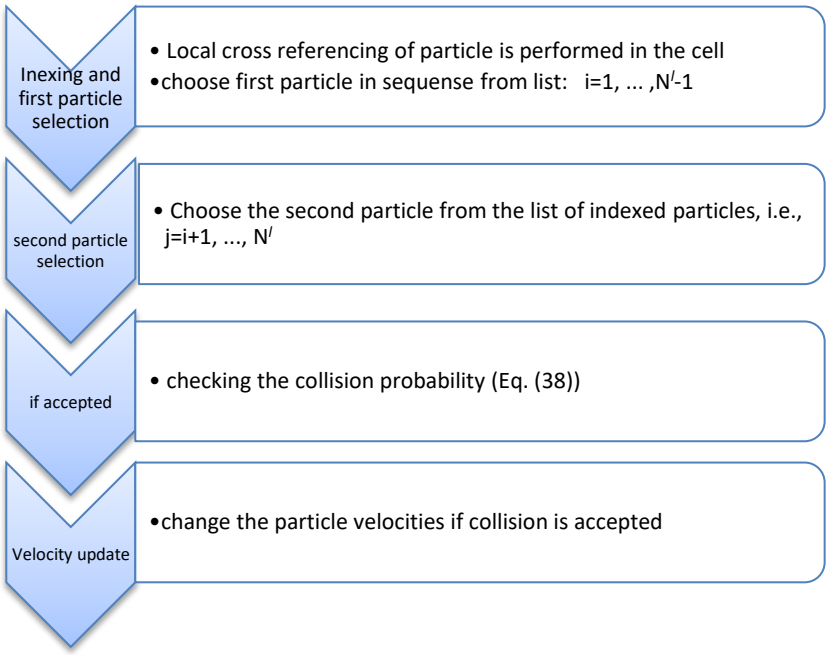

Fig. 9 BT collision procedure [9, 23-24]

3.5 Ballot Box collision scheme [9]

If the transition operator is approximated by a linear term in terms of *t* as:

$$G_3(t) = I + t \sum_{1 \le i < j \le N^l} w_{ij} \left(T_{ij} - I\right) \tag{39}$$

, the number of particle pairs is denoted by k= N(N-1)/2, and if one introduces the time step (*t*) inside the summation operator into the operator G_3(t), replacing tw_{ij} by $\frac{1}{\mathrm{k}}(ktw_{ij})$, then:

$$\mathrm{G_3(t)} = [1 - \sum_{1 \le i < j \le N^l} \frac{1}{\mathrm{k}}(ktw_{ij})]\mathrm{I} + \sum_{1 \le i < j \le N^l} \frac{1}{\mathrm{k}}(ktw_{ij})\mathrm{T_{ij}} \tag{40}$$

This form of operator G_3(t) can be interpreted in a straightforward way that lead to the Ballot Box collision model. The condition $P_{ij}\{ktw_{ij} > 1\} \ll 1$ should also be satisfied. In the Ballot Box scheme, the following procedure is performed one times for each cell (see Fig. 10):

a) At each time step, only a single pair of molecules is randomly selected with the probability of 1/k from the whole range of particles.

b) The possibility of collision is evaluated with the probability of $W_{ij} = ktw_{ij}$.

$$\mathrm{W_{ij}} = \frac{\mathrm{N(N-1)\sigma_{ij}g_{ij}t}}{2\mathrm{V^{(l)}}} > R_{nf} \tag{41}$$

If the collision was accepted, the velocities are upgraded to their post-collision values. The laboriousness of the scheme depends linearly on the number of particles, i.e., O(*N*). The problem with the Ballot Box scheme is that $t \ll \Delta t$ (Δt is the optimal time step of simulation) in order to fulfill condition $\{\mathrm{P}(ktw_{ij} > 1)\}$<<1. The collision algorithm Ballot-Box must be repeated m times in time step Δt, so that $\Delta t = mt$. As a result, within the time step Δt the scheme cannot prevent from repeated collisions.

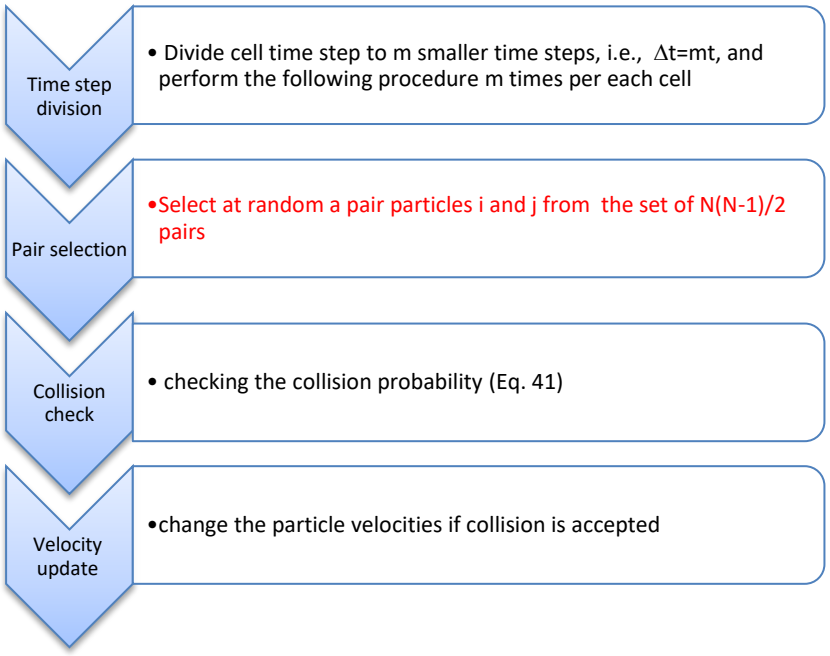

Fig. 10 Ballot Box collision procedure per each cell [9].

3.6 Null-collision (maximum frequency approach)

This method is first derived by Koura [16] for pseudo-Maxwellian gases and then extended and modified to arbitrary gases, σ(g) [10] (and called majorant frequency therein). In the Null-collision scheme, the maximum evaluation of the υ in (N, E, P) is computed in terms of $\upsilon_{max}(\mathrm{N},\mathrm{E},\mathrm{P})$. The collision operator T is replaced with $\mathrm{T}_{\max}$ while it keeps the condition of: $\upsilon_0(T_{max}-I)=\upsilon(T-I)$, therefore, the transition operator is written as follows:

$$\mathrm{G}_4(\mathrm{t})=\exp[t\upsilon_{max}(T_{max}-I)] \tag{42}$$

$$T_{max}=\left(1-\frac{\upsilon}{\upsilon_{max}}\right)I+\frac{\upsilon}{\upsilon_{max}}T \tag{43}$$

As the maximum value υ_{max} is a constant, $\mathrm{G}_4(\mathrm{t})$ defines a transition operator of a pseudo-Poisson process where the number of collisions are distributed according to

$$P_s(\upsilon_{max}t)=\frac{(t\upsilon_{max})^s}{s!}\exp(-t\upsilon_{max}) \tag{44}$$

Any pair selected for collision possibility has a collision chance of $\frac{\upsilon}{\upsilon_{max}}$ and collision rejection chance of $\left(1-\frac{\upsilon}{\upsilon_{max}}\right)$. Similar to Ballot-Box scheme and to introduce an equal opportunity for selecting a pair for collision, the maximum frequency value, w_{max} is computed. Values of υ_{max} and w_{max} are chosen such that: $\upsilon_{max}=kw_{max}$, where k is the number of particle pairs, then T_{max} is transformed to:

$$T_{max}=\sum_{1\le i\le j\le N}\frac{1}{k}\left[\left(1-\frac{w_{ij}}{w_{max}}\right)I+\frac{w_{ij}}{w_{max}}T_{ij}\right] \tag{45}$$

The numerical procedure of Koura's method is as follows:

Repeat the procedure below s-times [16]:

1- Compute maximum frequency as follows:

$$\upsilon_{max} = (\frac{1}{2})nN(S)_{max} \tag{46}$$

$$S_{max} = \sigma(g)_{max} \tag{47}$$

2- A random pair (i,j) is selected with the same probability from all particles.

3- The collision is accepted with the probability of $\frac{w_{ij}}{w_{max}}$, i.e., if $\frac{w_{ij}}{w_{max}} > R_{nf}$ collision is accepted.

4- Collisions are ended if summation of collision time (sampled from the Poisson distribution) exceeds the cell time step.

$$\sum_{n=1}^{s} \delta t_n \leq t < \sum_{n=1}^{s+1} \delta t_n, \tag{48}$$

$$P(\delta t > t) = \upsilon_{max}\, e^{-\upsilon_{max} t}$$

If υ_{max}=cte, this technique is one of the possible approaches to generate a Poisson random value $s(t)$. A classical algorithm for producing a random number from a Poisson distribution is developed by Knuth [56], as given in appendix 1.

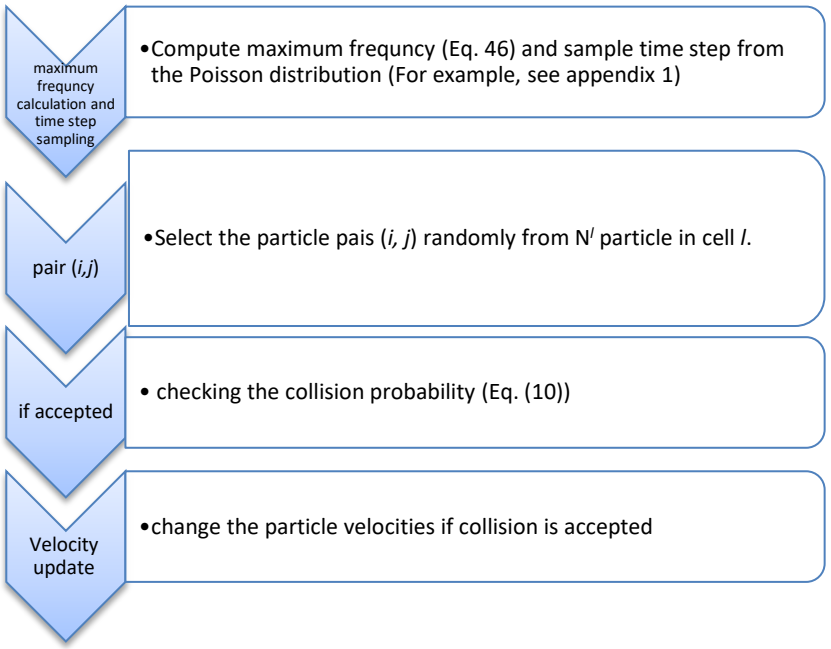

Fig. 11 Null collision procedure per each cell.

3.7 Simplified Bernoulli-trials

Bernoulli-trials (BT) scheme checks collisions with a given probability for all available collision pairs, i.e., N(N-1), which makes this algorithm quite time consuming, i.e. $O(N^2)$. Recently, Stefanov [23-24] showed that in small time-step intervals, it is possible to simplify the collision process and instead of checking all available possibilities, for the first selected as shown in BT particle, say *i*, one can choose randomly the second particle among the next sorted-particles in the list. Hence the number of selections would be reduced to (N-1) while theoretically the probability for collision of each pair remains unchanged based on the strict Markov process equal to the corresponding one in the BT method. Thus, in SBT each chosen particle pair is checked for collision only once within a time step and possibility of repeated collision is prevented while the computational costs are much reduced compared to the BT method.

As simplification, Stefanov showed that it is possible to extend the internal product in the right hand side of the $\mathrm{G(t)}$ (Eq. 22) in a series of *j* with respect to t to reach to a new simplified transition operator $\mathrm{G_5(t)}$ as follows [23]:

$$\mathrm{G_5(t)} = \prod_{\mathrm{i=1}}^{\mathrm{N^{(l)}-1}} [\left(1 - \sum_{\mathrm{j=i+1}}^{\mathrm{N^{(l)}}} \frac{1}{\mathrm{k}} (ktw_{ij}) \right) \mathrm{I} + \sum_{\mathrm{j=i+1}}^{\mathrm{N^{(l)}}} \frac{1}{\mathrm{k}} ((ktw_{ij})\mathrm{T_{ij}})] \tag{49}$$

, where $\mathrm{k} = \left(\mathrm{N^{(l)}} - \mathrm{i}\right)$. The algorithmic interpretation of operator $\mathrm{G_5(t)}$ states that instead of checking N(N-1) pairs (Note that the inner product in Eq. (33) considering all possible collision pairs N(N-1) is replaced here by a summation), it is possible in each acceptance-rejection, select the second collision particle at random and reduce the number of collision checking to (N-1). The SBT algorithm permits simulations with far less number of particles per cell compared to NTC, < N > ~ 1-2, where < > means mean value, and with reduced computational costs compared to BT algorithm. The numerical procedure of SBT is as follows: Particles in the l^{th} cell should be locally indexed to produce a particle list numbered as $1 \ldots N^l$. The first particle of the collision pair (*i*, *j*),

say *i*, is selected in sequence from the following particle list: $i = 1 \ldots N^l\text{-}1$. The second particle, say *j*, is chosen randomly with the probability of $1/k$ from $k = N^l - i$ particles taking place in the list after particle *i*.

$$j = (i + 1) + int(k \times R_{nf1}) \tag{50}$$

Each pair is then checked for collision with the probability, which with taking into account factor F_{num} and time step Δt reads

$$W_{ij} = \frac{(N_l - i)F_{num}\Delta t\sigma_{ij}g_{ij}}{V^l} > R_{nf2}. \tag{51}$$

It should be noted that the Δt should be adjusted so that in great amount W_{ij} does not exceed unity , say

$$prob\{W_{ij} \geq 1\} \to 0 \tag{52}$$

It is worth noting that the probability for $W_{ij} > 1$ should be kept always close to zero by choosing appropriate time step and cell size. The SBT procedure avoids the production of at least part of the eventually successively repeated collisions which occurs in the NTC scheme when it is applied with a small number of particles. More details of the theoretical background of this scheme are available in Refs. [23-24]. The sequence of SBT collision procedure is shown in Fig. 12.

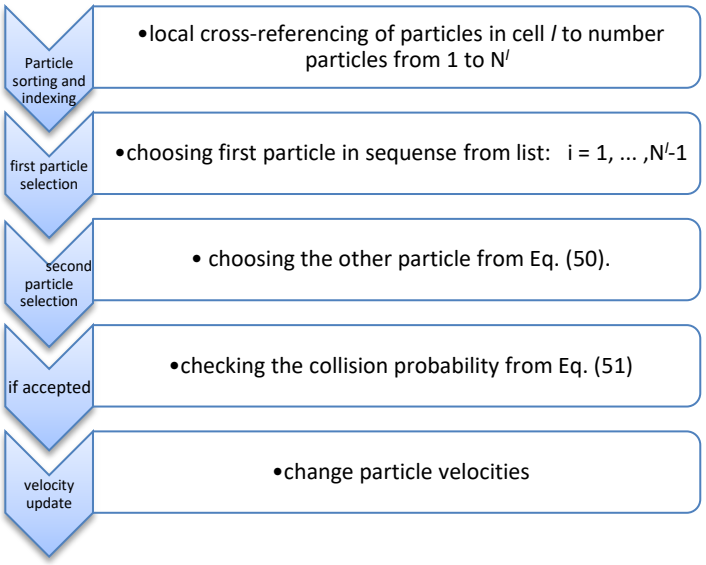

Fig. 12 SBT collision procedure per each cell

One of the benefits of SBT appears if one decreases cell size (dx) and time step (dt) without increasing the number of particles. Thus, this refines the simulation process when approaching closely the real process of molecular dynamic collision. The difference is only that SBT process is stochastic (random choice of the collision parameters). Simply, this process is localization of collisions more precisely with O(dx,dt) error. This process is not possible in NTC and NN methods because these algorithms always calculate a maximum number of collisions based on formula that estimate a gas in equilibrium and allows an estimation requiring a larger number of collisions. The situation with MFS scheme is better than NTC and NN, as there are not reminders in the estimation of real number of collisions with an integer, but all of these schemes assume a Poisson distribution of the collision pairs to be checked for collision. However, this idea does not work well when there are small number of particles because these schemes must to define preliminary a number of pairs (random or not) to be checked. Here it is possible the situation that the Poisson distribution or N_{coll} formula gives 5 pairs to be checked even when there are only 2 particles in the cell. Or Poisson distribution predicts one pair to be checked when there are 5 particles in the cell. This happens very often when there are small mean numbers of particle in the

cell. This gives considerable fluctuations in the collision process which leads to considerable errors in results.

3.7.1 A note on repeated collisions in SBT and NTC

The SBT procedure, as described in Sec. 3.7, prevents the possibility of repeated collisions in each time step. However, for possible repeated collisions in successive time steps that can occur in SBT there are two possible, one mathematical and other physical, answers. The mathematical answer is based on the fact that the SBT algorithm was derived from the Kac collision model assuming a strict Markov collision process within a time step [49]. The collision is based on its initial state, i.e., set of particle velocities in a cell at the beginning of each time step and the transition collision probabilities determined for each particle pair in a cell. After completing the collisions within a time step, a new state, i.e. velocity distribution is formed that is employed in the initial state for the collisions within the next step. At this moment, the step of particle free motion that changes the set of particles in the considered cell is neglected. It is obvious that the past of the collision history in a strict Markovian process is neglected. That is, the error realized by repeated collisions is included in the error of the Markov approximation of the collision process. Practically, the second answer is that first the exchange of particles between cells during the particle free motion occurs and then the probability of a collision of a given pair depends on the time step – the smaller time step leads to smaller probability for collision. The probability for a repeated collision is proportional to the product of pair probabilities. Therefore, it can be shown that the order of the events is $O(\Delta t^2)$. Since the accuracy of the splitting scheme is $O(\Delta t)$, one can neglect the repeated collisions as introducing an error of higher order for very small time steps. Altogether with the particle free motion step this allows to neglect the effect of the repeated collisions realized in successive time steps.

In the NTC and NN schemes, on the other hand, the situation is different, i.e., the decrease of time step leads to decrease of the maximum collision number in a collision cell within a time step. However, for a given particle pair the collision probability is determined by the acceptance-rejection rule with the probability given by Eq. (10) that does not depend on time step. Thus, the probability for a repeated collision of a twice chosen pair in the NTC algorithm does not decrease with the decrease of time step. That is why; NTC codes must introduce a preventing repeated collision rule within more time steps. However, the direct prevention of repeated collisions introduces extra errors in all schemes using the maximum collision frequency approach (NTC, MFS, Null-collision) when the number of particles per each cell is small. These schemes are based on the combination of acceptance-rejections procedure and the random choice of the particle pairs. When the number of particles is small, to complete the time step the collision procedure may check many times the same pair that previously was chosen and rejected. Next time the routine can choose the same pair and check it until a collision was realized. Using the direct prevention procedure, a conditional probability with removing from consideration some pairs destroys the correct random choice of pairs and the non-uniformity of probability distribution becomes significant. This leads to deviation from the correct probability, given in the Kac stochastic model for collision of each particle pair. This explains while the NTC, NN and MFS schemes cannot work accurately with small number of particles in cells. This point will be supported with the results presented in the following sections.

3.8 SBT on dual grids [24]

One reason for errors in the DSMC method stems from particles that are at a collision separation distance and have the potential to be selected as a collision pair, but they are not checked for collision as they are located in two neighboring cells. This difficulty may be overcome by using a dual grid (staggered grid) that is created by translation of cells (or subcells). This strategy improves the collision accuracy specially when there are a few particles per cell. For an

orthogonal grid, displaced grids are created by translating cells in each axis direction by a distance equal to a half-cell size. Figure 13 shows the formation of the displaced grid in structured cells. In this figure, solid lines show the main grid and dashed lines show the displaced grid that is obtained by displacing the main gird by a magnitude of $\Delta x/2$ in axial direction and $\Delta y/2$ in normal direction. It should be noted that the number of cells in the displaced grid is $(NCX+1)(NCY+1)$, where NCX and NCY are the number of cells in the original gird in x and y directions, respectively. The volume of internal cells in the displaced grid is equal to the volume of internal cells in the main grid. Nevertheless, the volume of boundary cells must be adjusted. Figure 13 also depicts two particles that in spite of being so close, they are not selected for collision as they are in two different cells in the main grid. After the grid is being displaced, these particles belong to one cell and possibility of collision will be checked. It should be noted that the numerical results obtained by using the dual staggered grid showed a slight improvement with regard to the space resolution compared to a single grid SBT application.

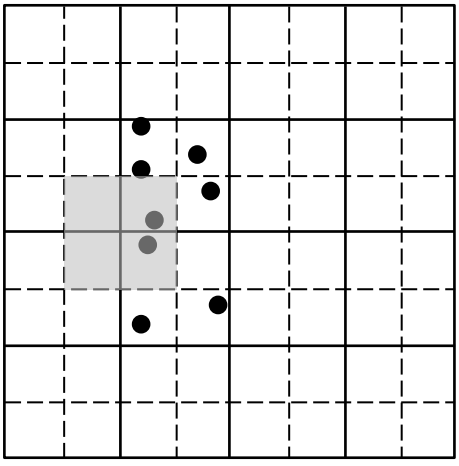

Fig. 13 Schematic of the displaced grid (dashed line): solid lines are the main grid, grey cell is a typical cell created after grid displacement. (copied with permission from Ref. [57])

3.9 SBT on transient adaptive subcells (SBT-TAS) [49]

Previous works [24] showed that computational efficiency of the SBT method decreases with increasing the number of particles in a collision cell. Using TAS technique, this problem may be avoided because the transient adaptive subcells are set dynamically in such a way that the number of particles always remains limited in every subcell. During the simulation, the particle distribution in cells is not uniform; therefore, there may be subcells which are empty or contain only one particle. In this case, no collisions are possible in such cells. In the NTC-TAS approach suggested by Su et al. [48], if such a case occurs, usually a search among the neighboring subcells is performed to find a partner for collision pair. It could be shown that there is no need to follow this procedure in the SBT-TAS algorithm. Instead, it is suggested to use a two-half-time-step collision algorithm and shift the transient adaptive subcell grid in the second half-time step in order to prevent the reduction of collision frequency in the cell. By using a dual subcell grid, the single particles in cells within the first half-time step will have the chance to find a collision partner within the second half-time step.

3.9.1 SBT-TAS: volume estimation on curved boundaries [30]

Unlike the NTC collision scheme, the collision probability function of the SBT scheme, Eq. 51, depends on subcell volumes, therefore, there is a necessity of having an accurate volume computation (approximation) of subcells in the SBT scheme. TAS divides the collision cell into equally spaced rectangular spaces, and the SBT procedure can independently operate within their space. By producing subcell divisions over a generally shaped collision cell, there are three types of subcell (Fig. 14-a):

(1) The first group is those which are out of the borders of the collision cell and they are not considered in the flow.

(2) The second group is those which are in flow but they are vacant, thus they are assumed inactive in the collision occurrence.

(3) The third group of subcells is the ones that are totally or partially in the flow and at the same time contain at least one particle. These subcells called as “in-flow active” subcells. They are the subcells that SBT could use them as the areas for performing a collision. In the probability function of the SBT scheme, Equation (51), V_l is the volume that is assigned to the particles. Since the collision cell is considered as a homogeneous space, Goshayeshi et al. [30] suggested that the cell volume is equally distributed among only in-flow active subcells (type 3). In regards of this definition, we can modify the probability function in the form of the Equation (53). For the l^{th} subcell, it will be:

$$W_{ij}^{l} = F_{num}\,(N_l - i)\,(\sigma g)_{ij}\,\frac{\Delta t}{V_l} \tag{53}$$

$$V_l = \frac{V_c}{NS_{type\ 3}} \tag{54}$$

, where w_{ij}^{l} is the collision probability of the pair (i,j) in the l^{th} subcell, N_l is the number of indexed particles for this subcell, $NS_{type\ 3}$ is the number of type 3 subcells, and V_l is calculated in a way that all the collision volume (V_c) is equally distributed among type 3 subcells. Corresponding to this volume propagation, Fig 14-b demonstrates how the cell volume is heterogeneously divided among the type 3 subcells. Eq. (54) could be substituted the direct calculation of the subcell volume, which could be relatively time consuming. This equation preserves a consistency with probabilistic nature of the DSMC method and is not limited to boundary cells, i.e., it could be utilized for all subcells in the simulation domain.

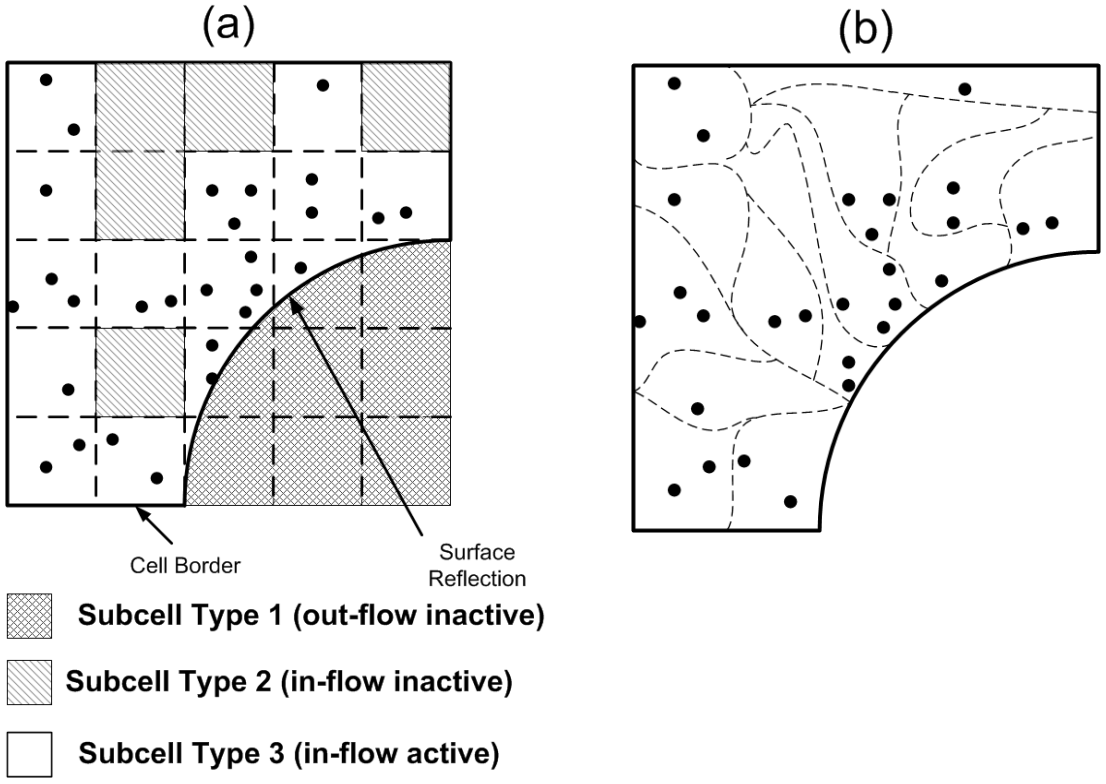

Fig. 14: Different subcell types produced around a circular cylinder (grey region); (a) rectangular subcell divisions for indexing particles, (b) subcell divisions based on the assigned volume in the estimation of probability function (divisions are tried to represent an equivalent volume of V_l) .

3.9.2 SBT-TAS: Time step interval control [30]

Previous investigation showed that there is a requirement of time step interval control at the subcell level [30]. There are some restricting rules on time step in the DSMC method, in both of motion and collision stages of particles. In this sense, any manipulation that violates these rules will result in errors. The SBT's features require that the TAS implementation to depend on the local parameters of the subcells. In fact, SBT cannot accept dependent TAS grids similar to NN or NTC does. This incapability comes from the nature of SBT, which force the scheme to determine the collision-frequency by investigating through binary considerations of particles, unlike other schemes that fulfill this task with one step estimation of the total number of collision events. Consequently, implementing TAS in SBT will produce the so called "subcells" as smaller collision cells, while the time step interval employed in these subcells are used from main cells.

This time step interval is calculated such that it produces a consistency between the allowed distances for the movement (transit time) and the allowed collision-frequency based on the mean collision time which has been determined in the main cell. Of course, there is no necessity that the mean collision time of the main cell and each of its subcells be the same.

Fig. 15 depicts this probable time variation in a series of subcells. In SBT-TAS implementation, all the subcells, S_1,…, S_5 has the same working-time-step equal to the main cell time-step ($Time_C$). Consequently, the subcell S_1 receives a larger time step than its actual value, while in case of S_2-S_5, they accept smaller values. In other words, the relation between the working-time-step and actual-time-step of S_1-S_5 subcells in relative to the $Time_C$ will be as follows:

$$Time\ step_{actual\ S1} < Working\ time\ step_{S1-S5} = Time_C < Time\ step_{actual\ S2-S5}$$

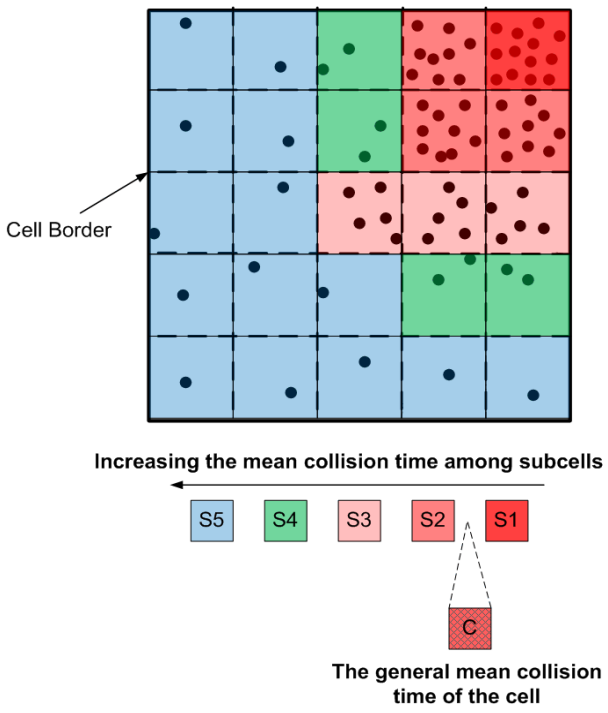

Fig. 15: Variation of the mean collision time among the subcells of a typical cell.

This phenomenon will be intensified if the considered cell is placed in complex regions such as shock interactions. In these situations, implementing SBT-TAS using collision cell time step will lead to a time-error, and the violations of DSMC's movement and collision decoupling will occur. In this state, those subcells that have a time step smaller than their actual value (S_2-S_5 subcells), will under-predict number of collisions. On the other hand, subcells that have a time-step larger than the actual value, subcell S_1, over-predict the number of collisions, while particle-transition paths are larger than the allowed amount. Consequently, violations of movement and collision decoupling will emerge in these subsets, see Fig. 16.

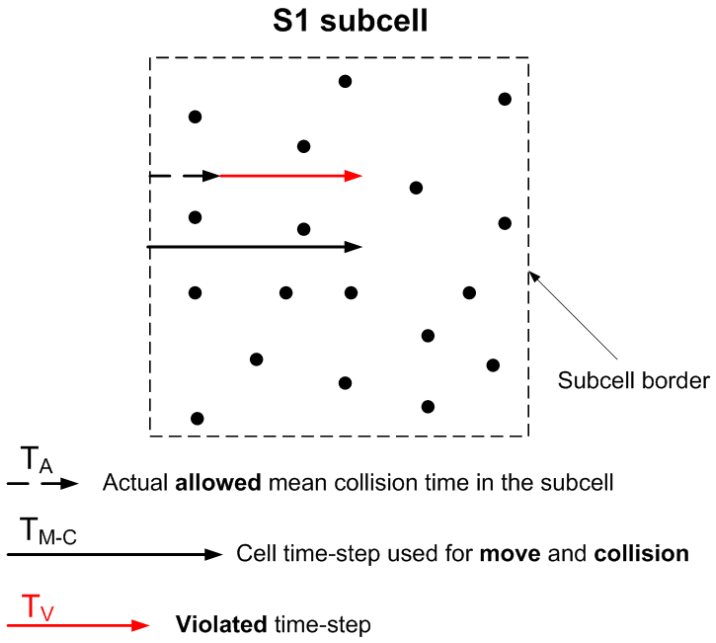

Fig. 16: S_1 subcell and time-step violation.

The violation time-scale, i.e., as called *Time-Slip*, $S_v = \frac{T_{M-C}}{T_A}$, is a constant that almost preserves its magnitude, even when the time-step of the cell (T_{M-C}) is being controlled in such a way that it becomes equal to the available smallest mean collision time among concurrent subcells of the collision cell. Therefore, any attempt to avoid this error by reducing the working time-step will be

unsuitable and it will just decrease the speed of the numerical procedure, while the S_v still exists in the cell space as a time-scaling factor.

In the SBT scheme, the acceptance-rejection depends on the value of the probability function (w_{ij}^{l}) of the two colliding particle pairs (i, j) in the l^{th} subcell. It is observed that the cells that are probable of containing S_1 subcells are mostly placed in the shock or shock-shock interaction regions. The sensible characteristic of these cells is that they have a heterogeneous distribution of particles within their space, which is a key factor in generating S_1 subcells. With increasing the usage of the TAS grid on these cells, the number of S_1 subcells will also increase. Hence, the TAS grid should be fabricated over these cells on such an extent that there would be no S_1 subcell. We assume that $W_{ij}^{l} > 1$ is a sign of the presence of S_1 subcells. Therefore, the controlling variable for each collision cell is defined as this:

$$C.V = \frac{N_E}{N_C} \tag{55}$$

, where N_E is the times that $w_{ij}^{l} > 1$ occurs and N_C is the number of collision occurrences. In fact, it is a ratio between the times that the probability function (w_{ij}^{l}) exceeds the acceptable limit to the all times that collision happens in that area, and at this work, it is also called as P-exceed ratio or P_E_R. Therefore, the implemented solution suggested in Ref. [30] is to enable the system to sense the degree of the generated error and secure it to a safe zone, where the threat of creation S_1 subcells is at the minimum state. At the same time, this solution should let the TAS system to work with its maximum capacity for the SBT scheme. This combination of SBT-TAS with this control mechanism is called as, “SBT-TAS C.M.”.

3.10 Intelligent SBT (ISBT)

The SBT collision scheme is designed to obtain correct collision frequencies with the minimum number of particles per cell. A modified version of this scheme, called intelligent SBT (ISBT) has

a semi-perception of inter-particle distances and is able to prioritize the acceptance of closer pairs, was suggested by Goshayeshi et al. [25]. The aim of developing of ISBT is to alter the particle sorting and acceptance-rejection process in the SBT scheme to bias the selections in support of closer partners. ISBT has two main stages. The aim of the first step is to define a smart way of locally indexing particles. The particle indexing should be modified in a way that a semi-perception of distance appears in the indexing process, i.e. in a collision cell with N_c particles, it should be an indexing method that satisfies the condition of ($\delta_i < \delta_j, 0 < i < j \leq N_c$), where δ_i is the distance of the i^{th} particle to a reference point ® (see Fig. 17-a). Investigations over the optimized location of the ® point exhibits that the indexed points, relative to their hierarchical order, would be closer to each other if the ® point is located on the corners of a rectangle that surrounds the particles (compare Figs. 17 (b-c)). Therefore, Goshayeshi et al. [25] suggested the random selection of cell/subcell corners to efficiently index particles quite close to each other. However, since the δ distance does not consider the angular distances, there are still some particles that are indexed successively while they are far from each other, specifically those particles on the opposite sides of the diagonal (e.g. particles 4 and 5 in the Fig. 17-c). Statistically, these particles are not the majority and, on the other hand, any other way for particle indexing would unavoidably produce situations that some indexed particles would be far from each other. It is crucial to note that while along the indexing direction (diagonal RB in Fig. 17-a) particles are prevented to collide in opposite corners (because they are indexed at the bottom and the top of the hierarchical order), along the other one (diagonal AC in Fig. 17-a) particles might be indexed as neighbors, and their collision, reverse the angular momentum associated with that collision pairs. Since these kinds of collisions might be inevitably supported in the ISBT scheme, as a solution, Goshayeshi et al. [25] suggested using elongated cell/subcells. In a quadrangular cell/subcell ('RABC' in Fig. 17-d) the maximum distance (*MD*) that two far-indexed particles could have is $\sqrt{2}$ times greater than the side length. However, using elongated cell/subcell obliges the time step

to be reduced accordingly. Therefore, in cases of hypersonic shock interaction simulations, Goshayeshi et al. [25] suggested using elongated cells/subcells with elongation factor of two ($m = 2$), while the time step is reduced about one third. Therefore, ISBT technique could be implemented alongside with the transient adaptive sub-cell technique (TAS) as described in Sec. 3.9.

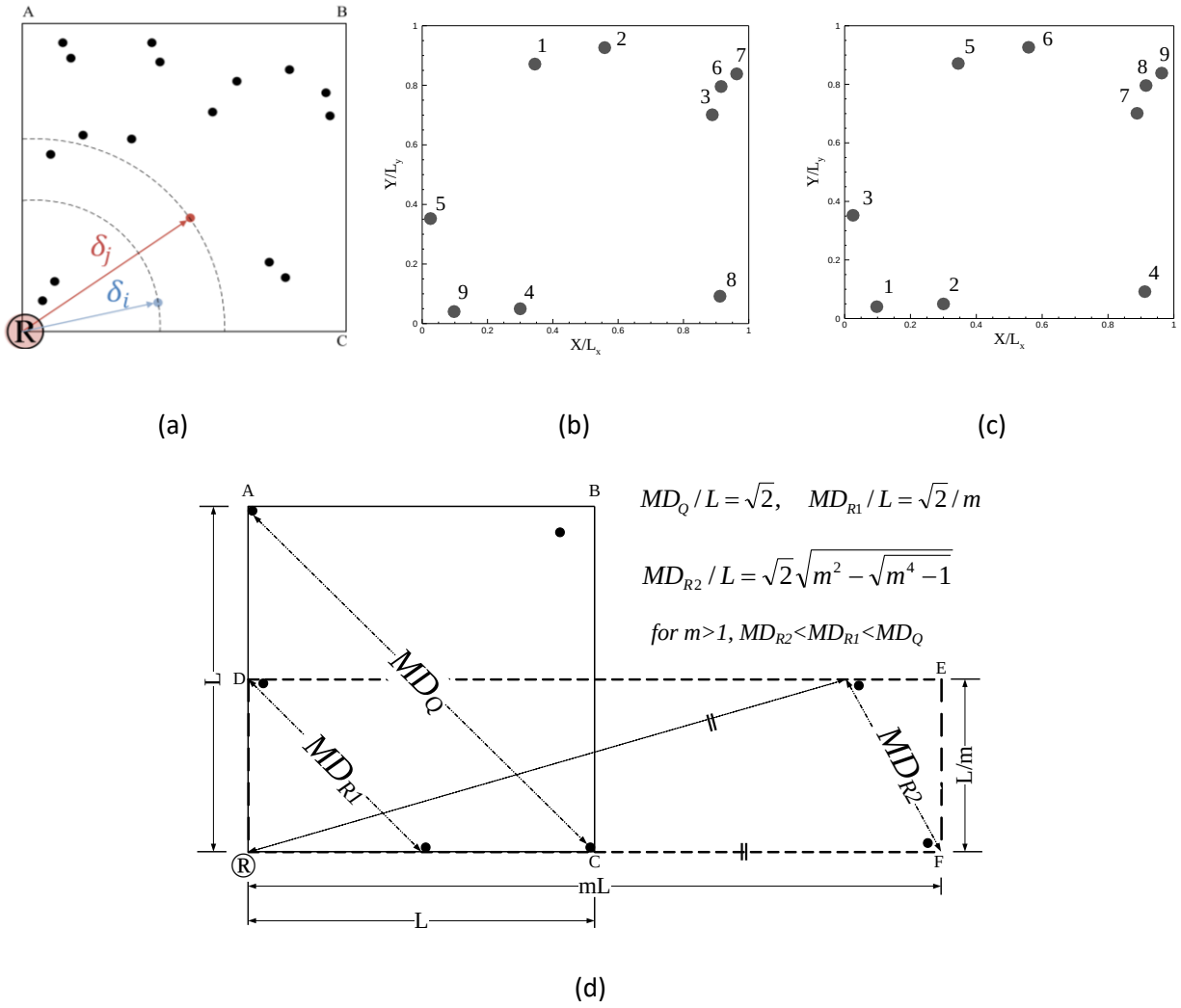

Fig. 17: Distribution of some particles in a cell/subcell; (a) a system of particle indexing based on the distance of particles to a definite center point ®, (b) the indexing results for a group of nine particles when the ® is located on the center of the cell, (c) when this point is on the left-down corner of the cell, and (d) the geometrical comparison between one quadrangle cell/subcell ("RABC") and its equal-area elongated cell/subcell ("RDEF"), while the calculated values for the maximum distance (*MD*) between two far-indexed particles are shown; they denote that elongated cell/subcell has smaller *MD* value.

The ISBT procedure could be implemented as follows:

The first particle, i.e. i, is sequentially selected from 1 to N_c, while its pair, i.e. j, at each sequent is randomly selected among the further indexed particles, according to the previous paragraph and following Eq. (50). The main difference with the SBT is that instead of regenerating the second random number (R_{nf2}), which was used in the acceptance-rejection section of the SBT scheme in Eq. (51), ISBT does not produce any new random number and implements the first generated one (R_{nf1}):

$$W_{ij} \geq R_{nf1} \tag{56}$$

, where W_{ij} is calculated through the Eq. (51). Figure 18 show the sequences of the ISBT procedures. As a result of this policy, pseudo-circular subcells (Fig. 19) will be created that allow an easier acceptance for closer available-pairs and a more difficult condition for further particles; it is because that smaller number for j, as the second particle in the hierarchical list of indexed numbers, is only obtained if the R_{nf1} is closer to zero, and conversely, greater number for j, as the second particle, is merely obtained if the R_{nf1} is further from zero.

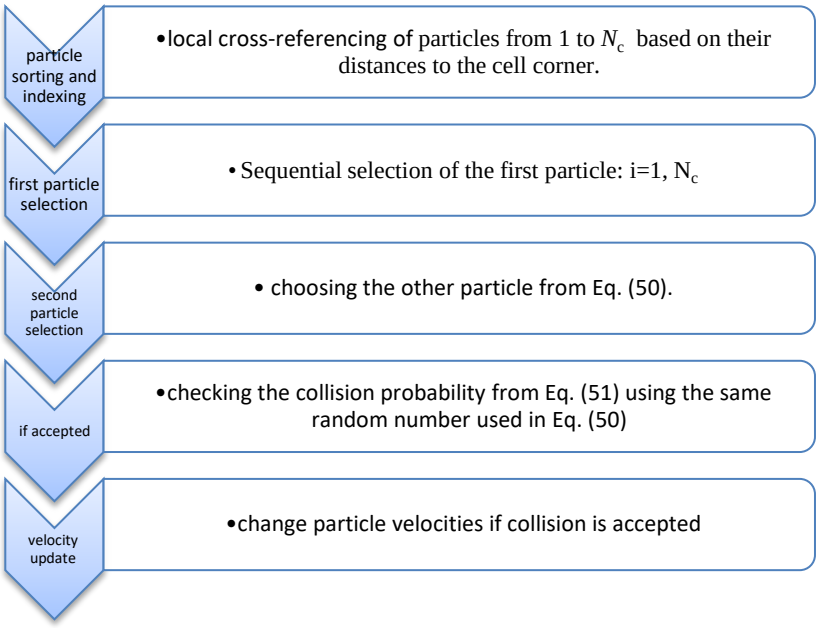

Fig. 18 ISBT collision procedure

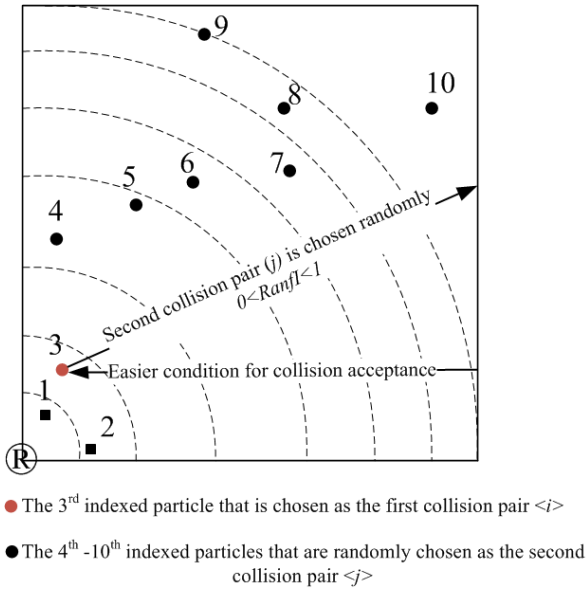

Fig. 19: Pseudo-circular subcells in the ISBT scheme that causes a biased selection for closer collision pairs. (Reprinted with permission from B. Goshayeshi, E. Roohi, and S. Stefanov, Phys. Fluids **27**, 107104 (2015). Copyright 2015 American Institute of Physics)

4. Validations of the SBT collision family

After presenting different collision algorithms in the framework of the DSMC method, this section presents a brief review of results obtained with the SBT collision family emphasizing the accuracy and suitability of this collision model for a wide spectrum of rarefied flow fields.

4.1 Collision frequency ratio from SBT-TAS and ISBT

The equilibrium collision frequency ratio of a cavity flow at $Kn = 0.005$, T_w=300 K, simulated on a 25×25 grid using SBT-TAS technique, is shown in Fig. 20 [49]. In this state, the theoretical equilibrium collision rate per molecule (CF_{th}) is given by [8]:

$$CF_{th} = 4nd^2 \sqrt{\frac{\pi K_B T_{ref}}{m_s}} \left(\frac{T}{T_{ref}}\right)^{1-\omega} \tag{57}$$

, where n, d, K_B, T_{ref}, m_s, and ω are number density, gas molecular diameter, Boltzmann constant, reference temperature, molecular mass, and viscosity-temperature exponent, respectively. CF_{num} represents the numerical value of this theoretical equilibrium collision rate that is calculated by the division of the number of collisions in each cell (N_{coll}) on the execution time ($Time$) and half of the mean particle numbers per cell (0.5 N_p):

$$CF_{num} = \frac{N_{coll}}{0.5\, N_p\, Time} \tag{58}$$

CF_{ratio} is the ratio of the CF_{num} to its theoretical value—given by Eq. (57)—it must have a magnitude close to unity. Using TAS and setting 2 particles per subcell, i.e., PPSC=2, 16×16 subcells were employed in each cell in average. As Fig. 20 shows, mean deviation of the equilibrium collision frequency ratio of one is in order of 10^{-4} and its maximum is about 0.2%. This proves that number of collisions in SBT-TAS scheme is accurate and coincides with the theory even using small number of particles per subcells (collision cells), i.e. two particles.

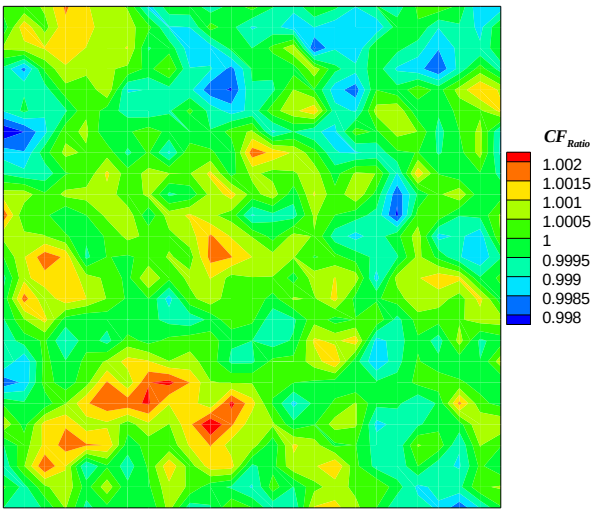

Fig. 20 SBT-TAS results for the equilibrium collision frequency ratio in the cavity using a 25×25 grid with 16×16 subcells per each cell and PPSC=2 [49].

The collision frequency of the ISBT scheme in an equilibrium state, for the argon flow in the cavity test case with U_{lid}= 0 m/s, Kn=0.01 and with surface and fluid temperatures have the same value of 273 K is evaluated using DS2V code [25]. Fig. 21-a, demonstrates the ability of the ISBT scheme to correctly predict the number of collisions, and Fig. 21-b, states that the deviation of the CF_{ratio} from the unity in the ISBT collision scheme, similar to the SBT scheme, is bounded with acceptable limit of 0.002. As the simulated cavity has diffuse reflecting walls, the eventual correlations cannot propagate at long distances

The dimensionless number, SOF, which is the mean collision separation distance (MCS) divided by the local mean free path (λ), is selected as a parameter for measuring the quality of collisions. Table 1 states that the ISBT, compared with the SBT collision scheme, reduced the SOF value quite considerably.

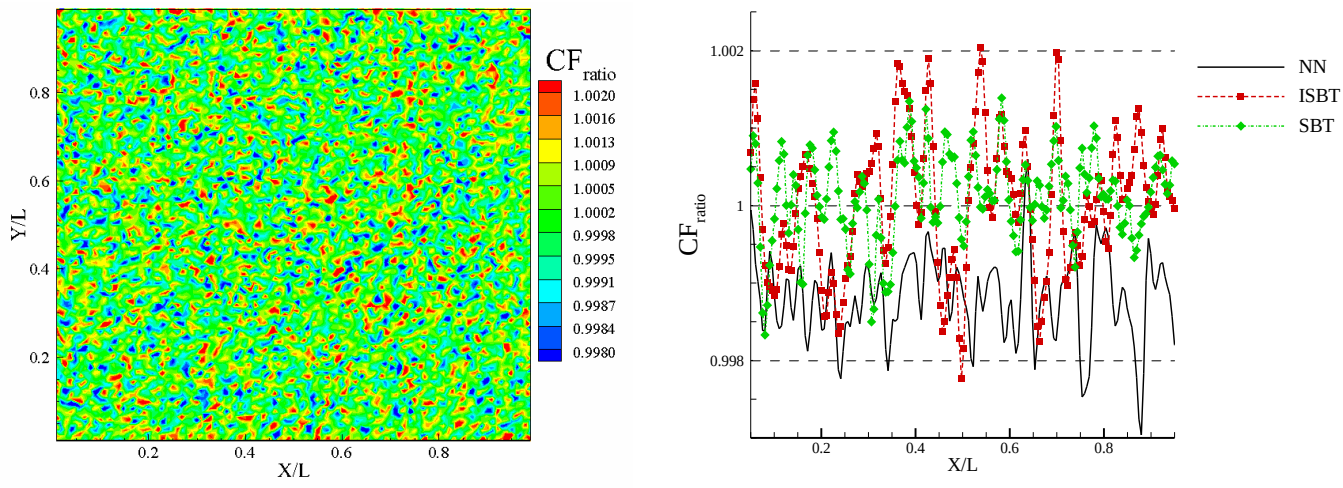

(a) (b)

Fig. 21: (a) contour of CF_{ratio} in the cavity at the equilibrium state, using the 100×100 grid and 10 particles per cell, calculated by the ISBT scheme, and (b) CF_{ratio} along the horizontal center line calculated by the NN, ISBT and SBT schemes. (Reprinted with permission from B. Goshayeshi, E. Roohi, and S. Stefanov, Phys. Fluids **27**, 107104 (2015). Copyright 2015 American Institute of Physics)

Table 1: Comparison of the $SOF = (\frac{MCS}{\lambda})$ value in the lid-driven cavity flow between NN, ISBT and SBT collision schemes. (Reprinted with permission from B. Goshayeshi, E. Roohi, and S. Stefanov, Phys. Fluids **27**, 107104 (2015). Copyright 2015 American Institute of Physics)

Collision scheme	*Division size in DS2V code*	*SOF value*	*SOF normalized by the NN value*	*SOF normalized by the SBT value*
NN	100-100	0.0477	1	0.182
ISBT	100-100	0.1740	3.66	0.666
SBT	100-100	0.2621	5.49	1

4.2 Fourier flow: comparison with theory

The convergence behavior and accuracy of the DSMC technique for Fourier problems for near-continuum conditions was investigated for the NTC method [58-59]. A similar evaluation was made for the SBT method [60]. The hard-sphere argon was simulated at the reference pressure

and temperature: $P_{init}=P_{ref}= 266.644\times10^{-5}$ Pa and $T_{init}=T_{ref}=273.15$ K, and Kn=0.0237. Fig. 22-a shows that the Sonine-polynomial coefficients a_k/a_1 for k=2,3 obtained from the DSMC away from walls agree with the theoretical value for NTC and SBT with a few particles per cell. Fig. 22-b compares the heat conductivity ratio (theoretical to DSMC) from NTC and SBT solutions and show that both numerical solutions agree with each other.

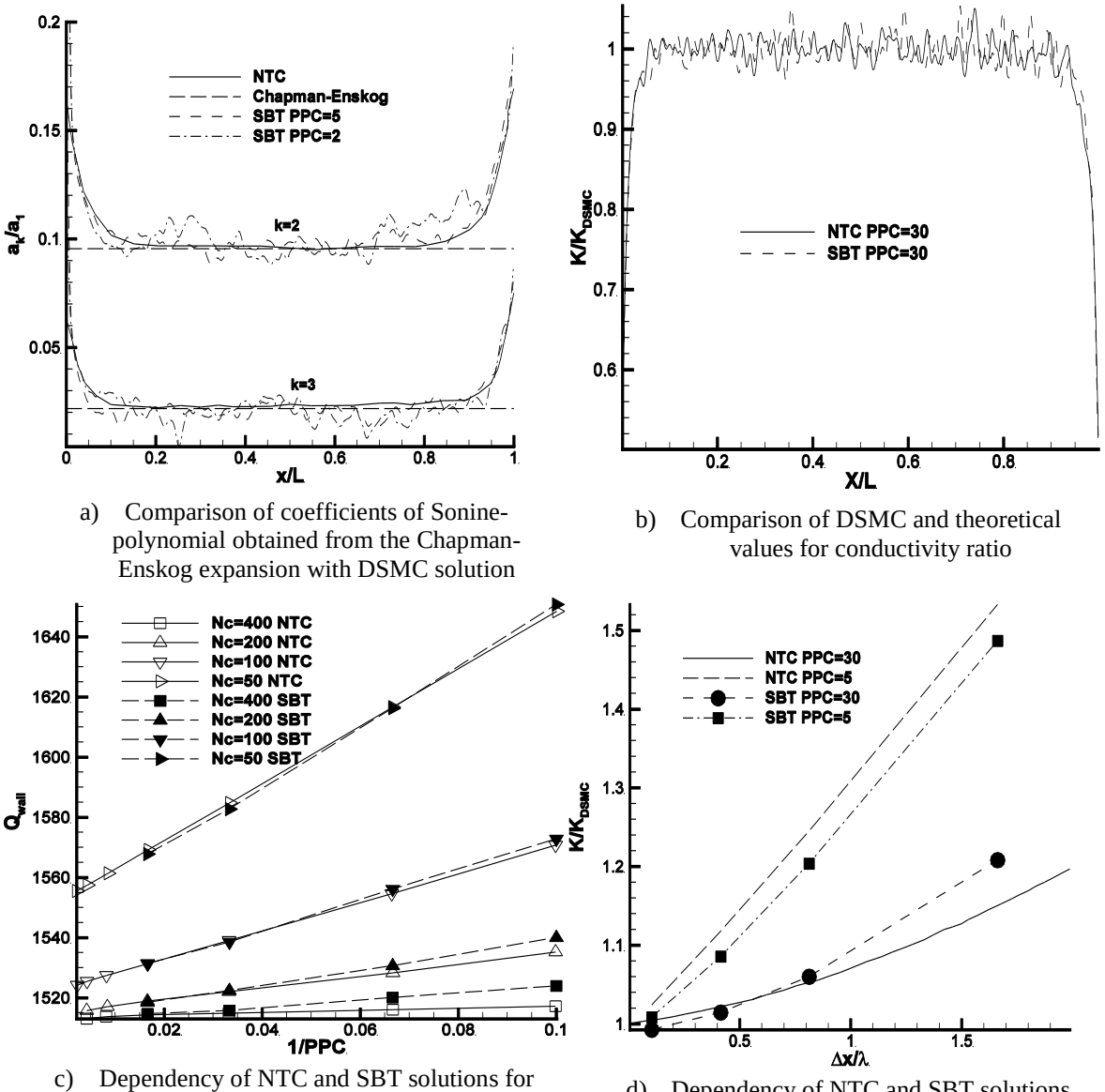

a) Comparison of coefficients of Sonine-polynomial obtained from the Chapman-Enskog expansion with DSMC solution

b) Comparison of DSMC and theoretical values for conductivity ratio

c) Dependency of NTC and SBT solutions for the wall heat flux on the cell size (N_c) and PPC.

d) Dependency of NTC and SBT solutions for the conductivity ratio on the cell size

Fig. 22: (a) Comparison of SBT and NTC solution methods for Fourier flow.

Fig. 22-c compares dependency of the SBT and NTC solutions for the wall heat flux on the number of particles per cell (PPC) and cell size. Both solutions agree with each other, however, SBT used a smaller time step. Fig. 22-d compares the dependency of NTC and SBT solutions for the conductivity ratio on the cell size, for both of the investigated PPC's, SBT and NTC solutions for the conductivity ratio approach to unity as cell size reduces.

4.3 Cavity flow

The SBT solution was compared with the NTC and MFS methods for the cavity geometry at Kn=0.005 and a moving lid at the velocity of $U_{lid} = 100\, m/s$ and $10\, m/s$ [57]. Cavity flow is considered as a classical test case for DSMC solvers [61-67]. Variable hard sphere (VHS) model of the monatomic argon, m=6.63×10^{-26} Kg and d=4.17×10^{-10} m was considered as the gaseous flow. Using a 400 × 400 grid cells, the minimum required particle per cell was investigated for the NTC scheme. As Fig. 23 depicts temperature on the centerline of the cavity, $< N > = 20$ (< > means average) could reasonably provide the sufficient accuracy for the NTC scheme. Fig. 24 compares temperature in the vertical centerline from the NTC with the SBT and MFS solutions. The figure indicates that the only scheme which provide accurate results with N=2 is the SBT scheme.

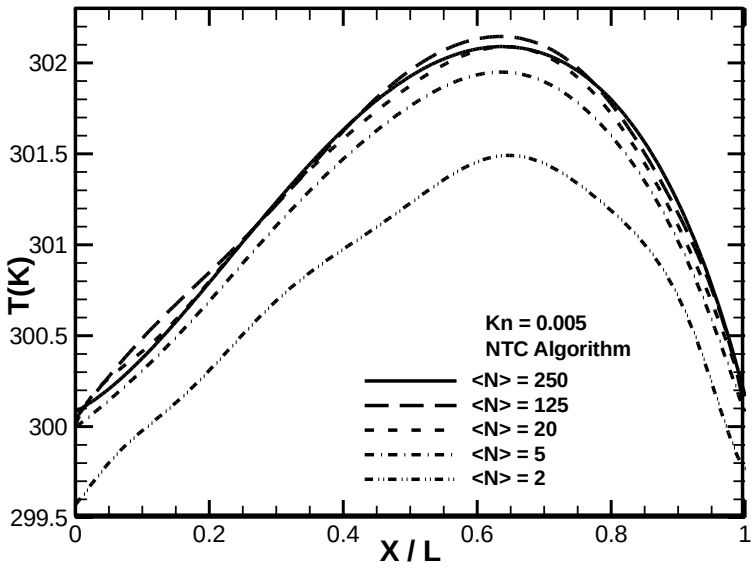

Fig. 23 Effect of number of particle per cell on the accuracy of the NTC collision scheme in prediction of temperature field in the horizontal centerline of the cavity. (reproduced with permission from [57])

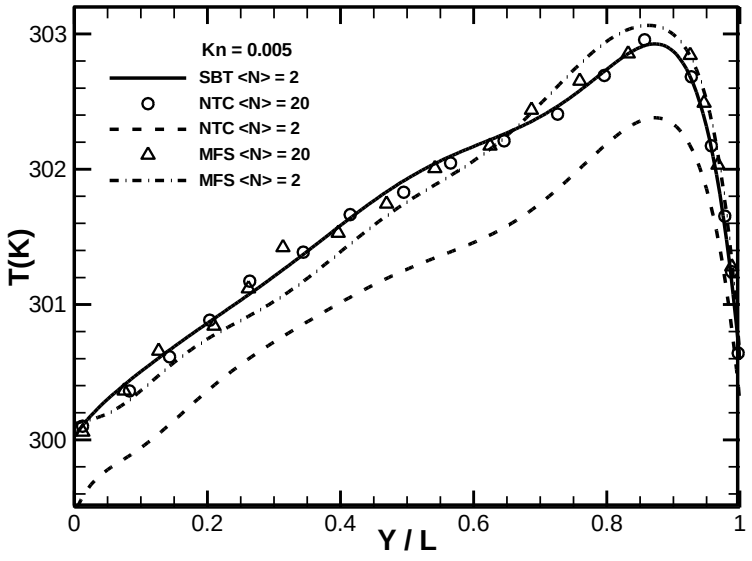

Fig. 24 Comparison of the SBT, MFS and NTC schemes in prediction of thermal pattern in the vertical centerline of the cavity. (reproduced with permission from [57])

Table 2 compares the required relative computational time of the SBT and NTC schemes for the cavity flow. The figure shows that SBT scheme with two particles requires less computational

time compared with the NTC solutions with 5 and 20 particles per cell, while the NTC needs around 20 particles per cell to predict accurate solutions, as shown in Fig. 23.

Table 2. Relative computational time for cavity flow. (reproduced with permission from [57])

	<*N*>	*time*
SBT	2	0.79
NTC	250	1.15
	125	1.07
	20	1
	5	0.98
	2	0.75

For the case of Kn=0.005, T_w=300 K and U_{lid}= 100 m/s, 25×25 grid, PPC=512 and PPSC=2, solution of the SBT on dual grid (SBT-Dual) is compared with the SBT-TAS and NTC solutions, the latter here called correct solution and is obtained on a 200×200 grid with 2 fixed subcells in each direction and 20 particles per cell [49]. Since the employed grid is coarse, it is quite expected that if we do not employ TAS, incorrect SBT solution will be attained, as is shown in Fig. 25, which depicts velocity components and temperature profile on the horizontal axis of the cavity. The figure shows that using dual grid does not improve the accuracy of the SBT-TAS solution more. Fig. 26 compares SOF from the SBT-Dual, SBT-TAS and SBT-TAS-Dual. The figures shows that using TAS drastically reduced the SOF, and use of dual grid reduced the SOF by half, however, had not any impact of the accuracy because the respective SOF was almost below 0.3, the minimum value that Bird stated could guarantee accuracy of solutions [13].

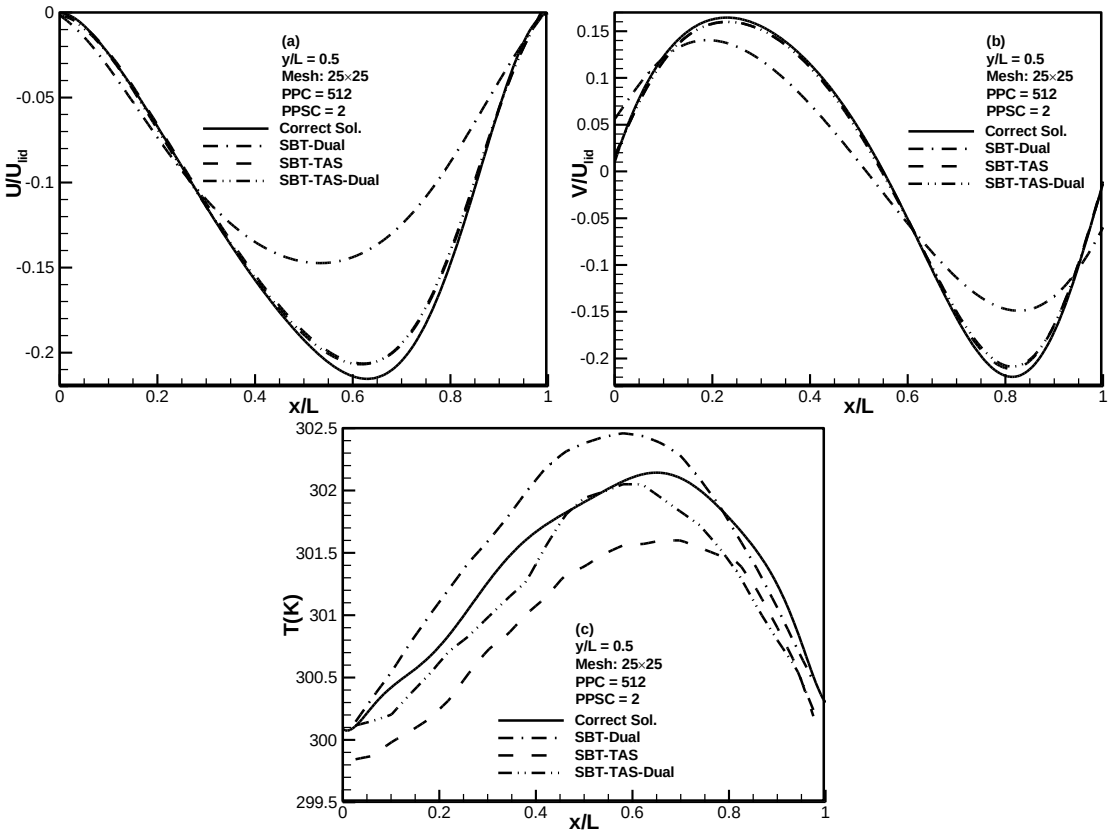

Fig. 25 Results of the TAS technique on the horizontal axis of the cavity obtained using 25×25 grid-PPC=512, PPSC=0.5 [49]

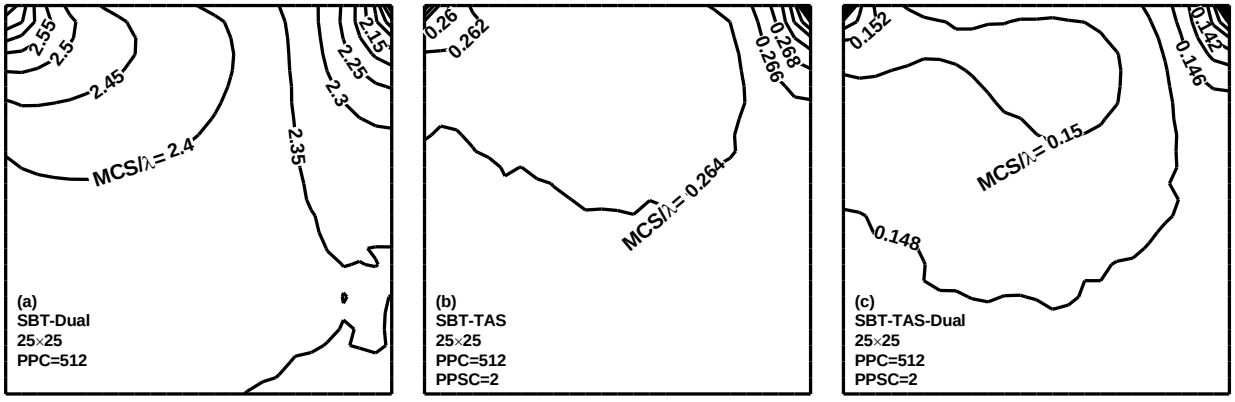

Fig. 26 SOF (MCS/λ) in the cavity flow
(a) SBT without applying TAS (b) SBT-TAS (c) SBT-TAS-Dual [49]

4.4 Flat plate flow

Hypersonic flow over a small scale plat of length 90 nm with the surface temperature of $T_{wall} = 500K$, Kn= 0.01 and T_{in}=300 K was considered as a test case for the SBT, NTC, MFS and SBT-TAS schemes [57]. The effect of number of particles per each cell is depicted in Fig. 27, where the figure indicates that both of NTC and MFS schemes require around 20 particles per cell to predict particle independent results while the pure SBT scheme works well even with one particle per cell in this case, i.e., sensitivity of the SBT solution to the PPC is quite low.

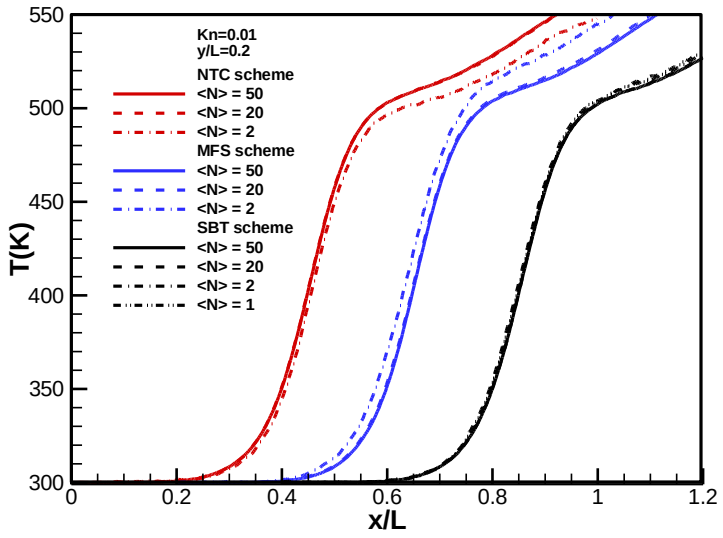

Fig. 27 Effect of average number of particles per cell on the accuracy of the temperature profile at y/L=0.2 for the flat plate case. Profiles are shifted to right for MFS and SBT schemes to make differences more clear. (reproduced with permission from [57])

Fig. 28 compares effect of using TAS on improving the SBT results over a coarse grid of 70×42 cell with PPC=28 and PPC=2. The figure shows that results without using TAS are inaccurate while use of TAS make the SBT solution as accurate as benchmark case, obtained on 370×222 grid and PPC=20 using NTC. Fig. 29 also indicates that use of TAS considerably decreases SOF compared to no-TAS case.

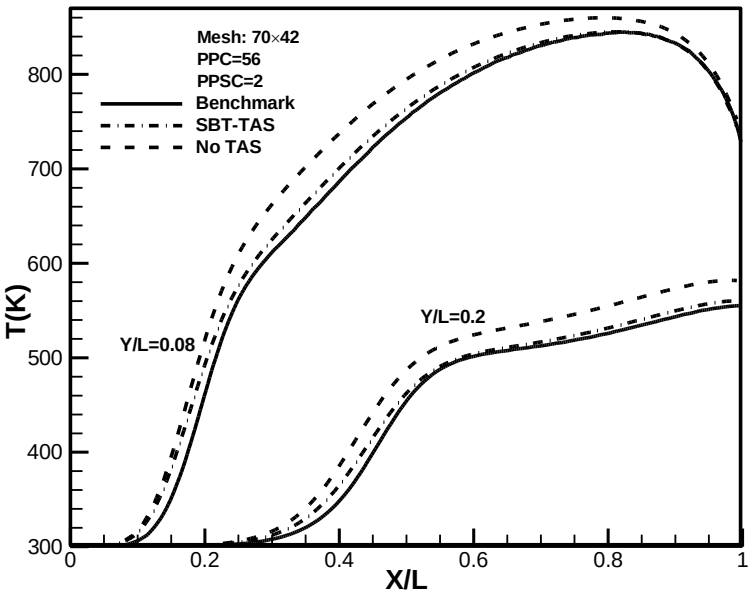

Fig. 28 Effect of using TAS technique for improving the results in 70×42 grid with PPC=56 and PPC=2 along the lines $\mathrm{Y/L} = 0.08$ and $\mathrm{Y/L} = 0.2$

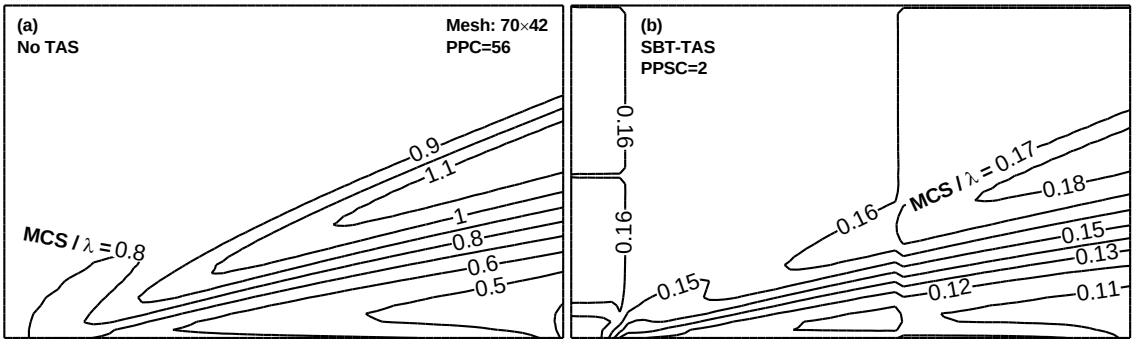

Fig 29. Effect of using TAS on decreasing $SOF = \mathrm{MCS}/\lambda$ for the flat plate flow;
Grid: 70×42, (a) without TAS (b) with TAS.

4.5 Rarefied flow past an airfoil

Rarefied supersonic and subsonic gas flow around a small-scale NACA 0012 airfoil was simulated using SBT and collision scheme [68-69]. The small-scale airfoils are widely employed in micro-air-vehicles. Flow field is investigated at Mach=2, Kn=0.26 and α=45°. Fig. 30 shows distribution of pressure coefficient and normalized slip velocity on the airfoil surface obtained using different values of PPC using SBT. In this case, the figure well indicate that SBT could provide accurate solution using even PPC=1. In addition, SBT solution shows almost no variations, expect statistical noises, in results with the changes in PPC. Figures 30-c-d compares the normalized density from the DSMC solution with the experimental contour provided in Refs. [70-71]. The figure shows a suitable agreement between the numerical and experimental data.

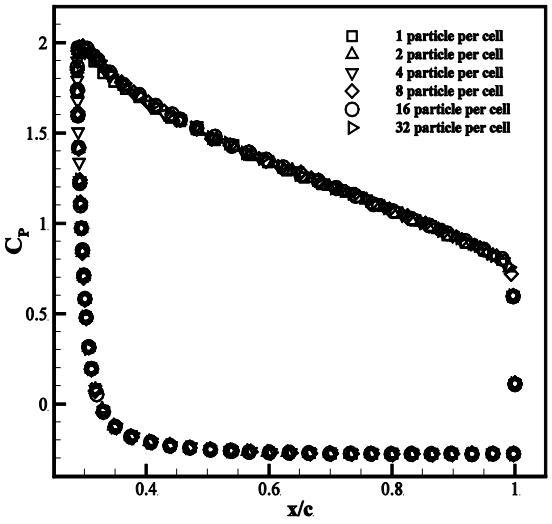

a) C_p distribution

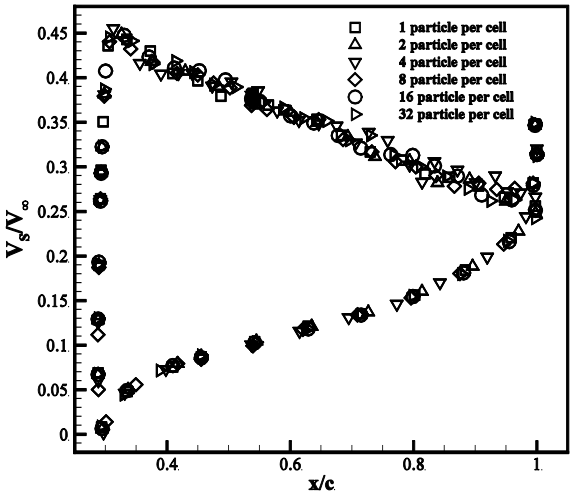

b) Normalized slip velocity

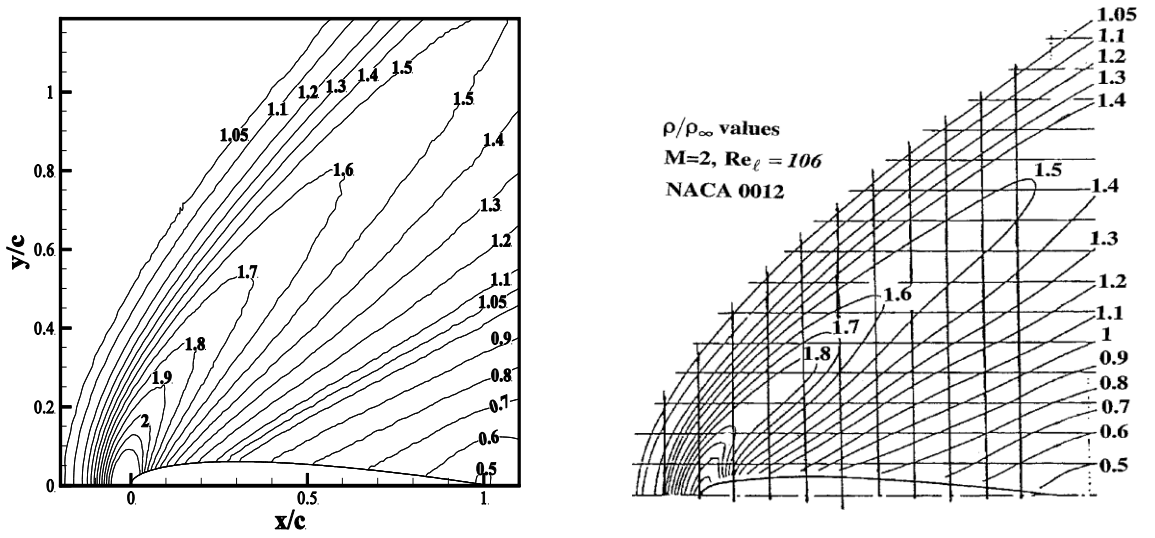

c) SBT solution for normalized density

d) Experimental picture for airfoil density [70-71]

Fig 30. Flow field investigation around an airfoil using SBT collision technique [68].

4.6 Micro and nano Nozzle flow

Flow inside micro and nano nozzles has been of interest of various researchers, see [72-75]. Accuracy of the SBT technique in treating rarefied micro and nano scale nozzle was considered [76]. Nitrogen flow with an inlet Knudsen number of $Kn_{inlet}=7.781\times10^{-4}$ was considered. Fig. 31 shows that SBT technique using PPC=2 at the steady state condition could provide particle independent results. Fig. 32 compares Mach number contours inside the micronozzle using both of SBT and NTC schemes, where both solutions show a good agreement. It should be noted that NTC needs PPC=10 to provide accurate solutions for all flow properties inside the nozzle.

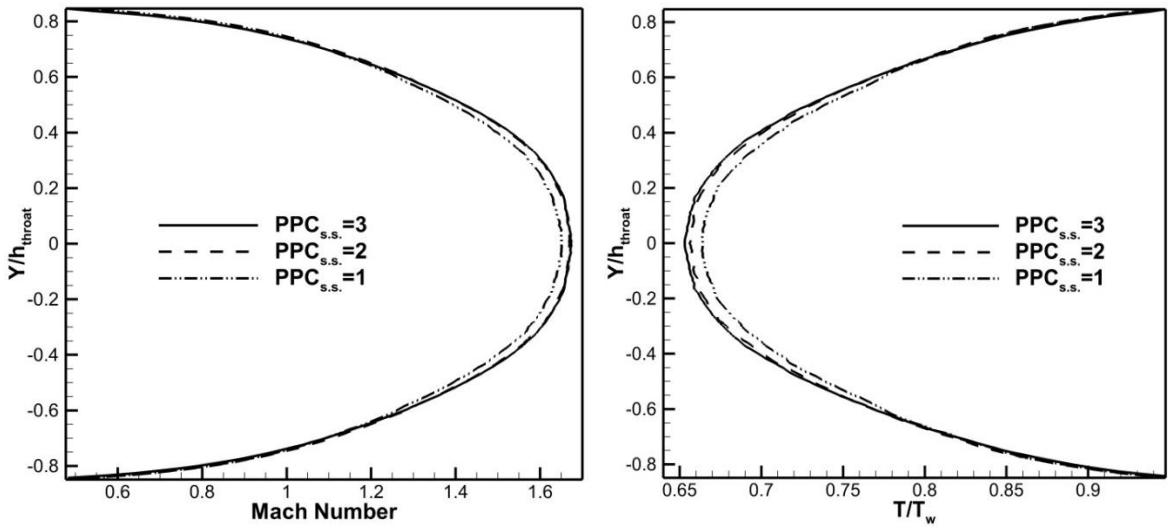

Fig. 31 Particle dependency of the SBT scheme for (a) Mach number, (b) normalized temperature at the nozzle exit [76].

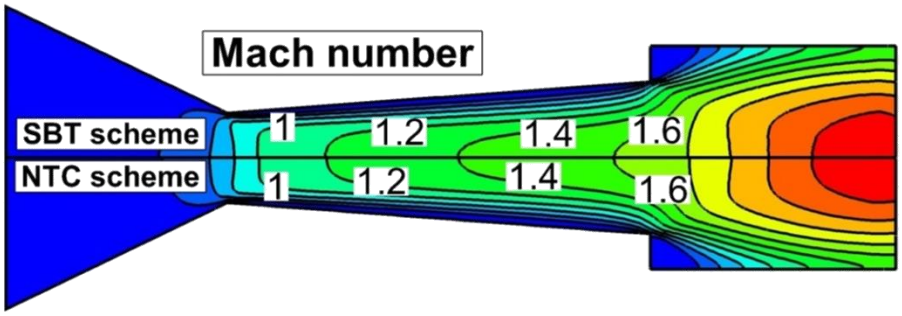

Fig. 32 Comparison of SBT and NTC techniques for Mach number contours inside the micronozzle [76].

4.7 Hypersonic flow over cylinder and biconic geometry

Hypersonic flows over the cylinder and biconic geometry are famous test cases in rarefied gas dynamics considered by various researchers to evaluate their DSMC solvers and algorithms [77-84]. Goshayeshi et al. [25, 30] evaluated the performance of the SBT, SBT-TAS and ISBT techniques in treating rarefied hypersonic flows. For the cylinder case, Mach 10 (2634.1 m/s) flow of argon at T=200 K passing over a 12 inch circular cylinder with a fully diffusive surface at T_s=500 K and a nominal free-stream Knudsen number of 0.01 is considered.

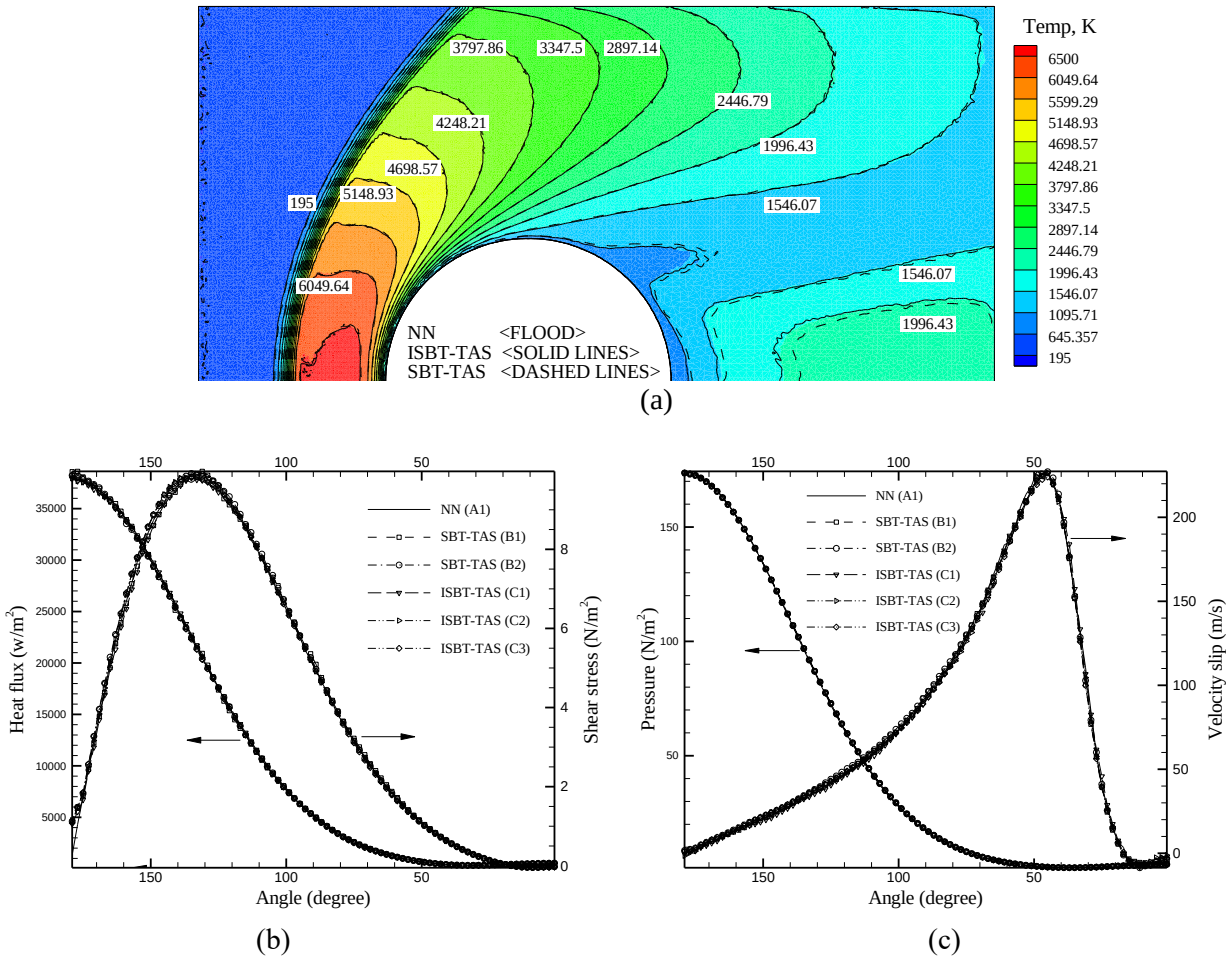

Fig. 33: a) Comparison of the temperature contour from NN, ISBT-TAS, and SBT-TAS b-c) Comparison of surface properties (heat flux, shear stress, pressure, slip velocity) in the cylinder flow problem (Reprinted with permission from B. Goshayeshi, E. Roohi, and S. Stefanov, Phys. Fluids **27**, 107104 (2015). Copyright 2015 American Institute of Physics)

Fig. 33-a shows a comparison of temperature contour around the cylinder from NN, ISBT-TAS, and SBT-TAS techniques. All SBT solutions match NN solution; however, ISBT matches the NN solution in the wake region much better. Figs. 33-b-c compares surface properties (heat flux, shear stress, pressure, slip velocity) over the cylinder. For all investigated properties, there is an excellent agreement between the SBT family results and those of NN.

Hypersonic nitrogen flow of Mach 15.6 passing over a 25°-55° degree biconic geometry is a quite complex test case for numerical schemes as it consists of a laminar recirculation zone, laminar

expanding zone, high-speed low-density region, and low-speed high-density region [80-84]. Fig. 34 shows the biconic and structure of different shock interactions occurred over this geometry.

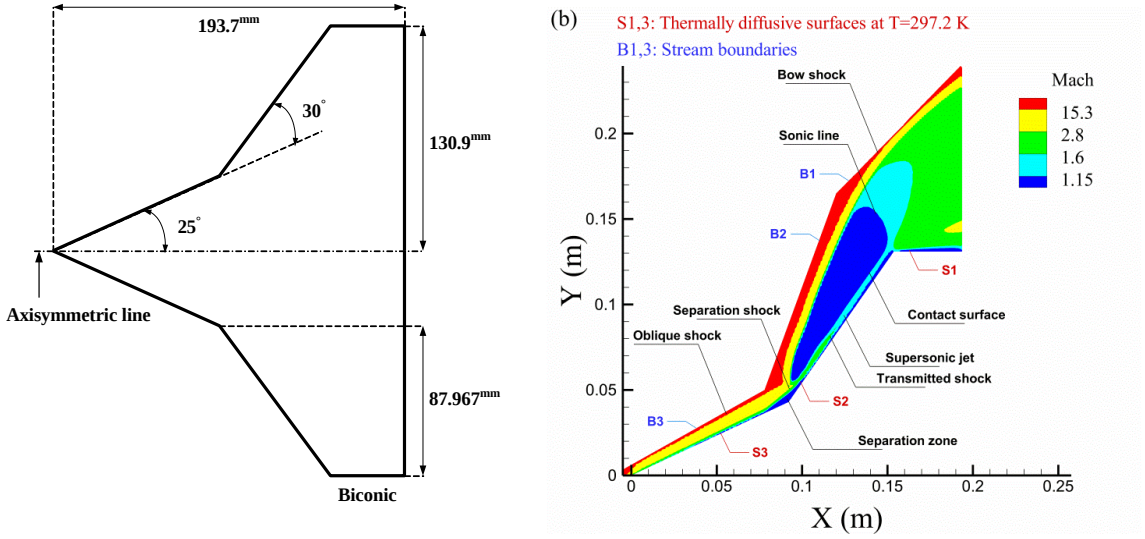

Fig. 34: Biconic geometry (left) and shock structures (right) around the geometry obtained by DSMC (Reprinted with permission from B. Goshayeshi, E. Roohi, and S. Stefanov, Phys. Fluids **27**, 107104 (2015). Copyright 2015 American Institute of Physics)

A comparison of the heat flux and pressure distribution over the biconic geometry, from SBT-TAS, ISBT-TAS, NN and experimental data is shown in Fig. 35. Fig. 36 shows contour of temperature and SOF from ISBT-TAS and NN over the biconic surface. All numerical solutions show almost a suitable match between ISBT-TAS and NN.

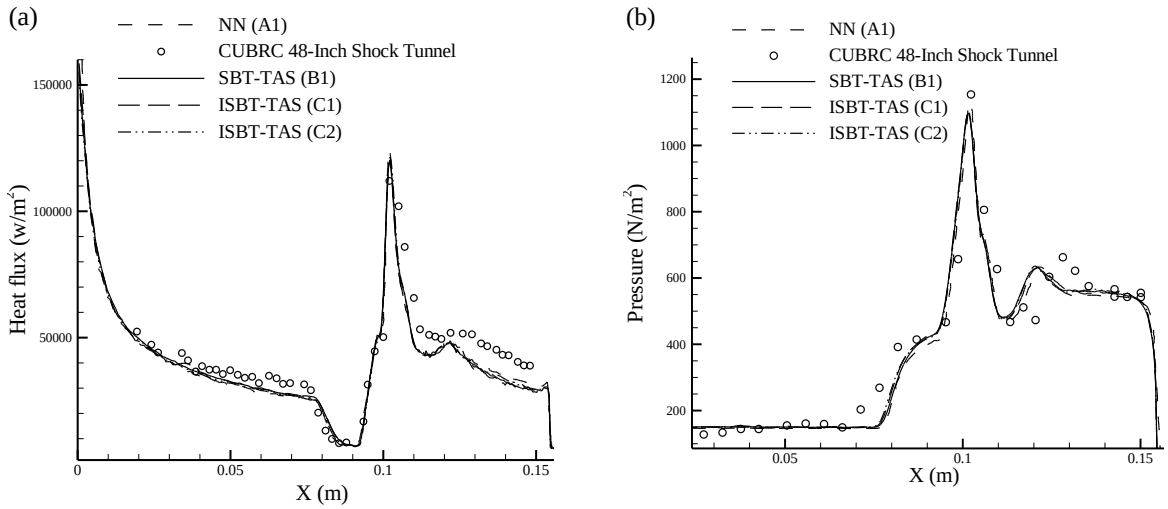

Fig. 35: Comparison of heat flux and pressure distribution around the biconic geometry from different DSMC models, (Reprinted with permission from B. Goshayeshi, E. Roohi, and S. Stefanov, Phys. Fluids **27**, 107104 (2015). Copyright 2015 American Institute of Physics)

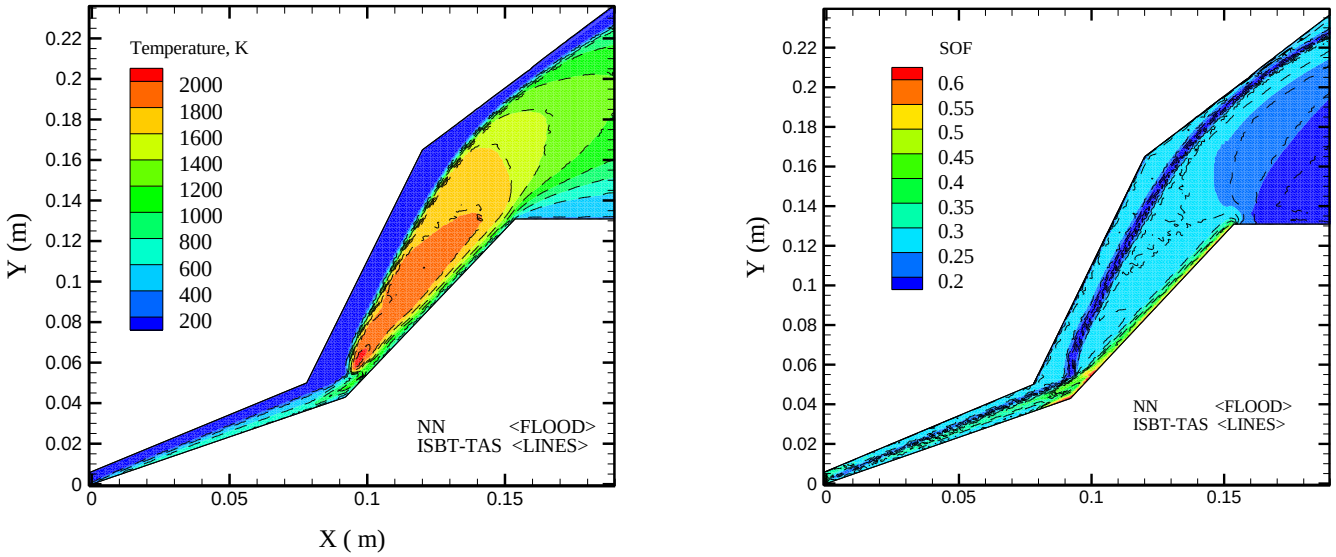

Fig. 36: a) Comparison of ISBT-TAS and NN collision schemes in treating hypersonic external flow over biconic, a) temperature contours, b) contours of SOF (Reprinted with permission from B. Goshayeshi, E. Roohi, and S. Stefanov, Phys. Fluids **27**, 107104 (2015). Copyright 2015 American Institute of Physics)

4.8 Re-entry test case with chemical reactions [85]

The SBT-TAS and NN collision models are applied to treat a typical hypersonic atmospheric re-entry problem exposing to dissociation and recombination chain reactions of real-air. The Total Collision

Energy (TCE) [86-87] model, with reactions listed in Table 3, is used to simulate chemical reactions in both collision schemes of NN and SBT-TAS. Fig. 37-a shows the schematic of the re-entry geometry and also indicates investigated working conditions. Fig. 37-b shows temperature contours from both SBT-TAS and NN scheme, with suitable agreement expect small differences in the wake region. Figs. 37-c-d compares temperature jump and species distribution over the surface, with an almost reasonable agreement between both schemes.

Table 3: The employed chemical reactions in the investigated test case.

No.	Reactions
Dissociation/Recombination reactions	
1	$O_2+N \leftrightarrow O+O+N$
2	$O_2+NO \leftrightarrow O+O+NO$
3	$O_2+N_2 \leftrightarrow O+O+N_2$
4	$O_2+O_2 \leftrightarrow O+O+O_2$
5	$O_2+O \leftrightarrow O+O+O$
6	$N_2+O \leftrightarrow N+N+O$
7	$N_2+O_2 \leftrightarrow N+N+O_2$
8	$N_2+NO \leftrightarrow N+N+NO$
9	$N_2+N_2 \leftrightarrow N+N+N_2$
10	$N_2+N \leftrightarrow N+N+N$
11	$NO+N_2 \leftrightarrow N+O+N_2$
12	$NO+O_2 \leftrightarrow N+O+O_2$
13	$NO+NO \leftrightarrow N+O+NO$
14	$NO+O \leftrightarrow N+O+O$
15	$NO+N \leftrightarrow N+O+N$
Exchange reactions	
16	$NO+O \leftrightarrow O2+N$
17	$N2+O \leftrightarrow NO+N$

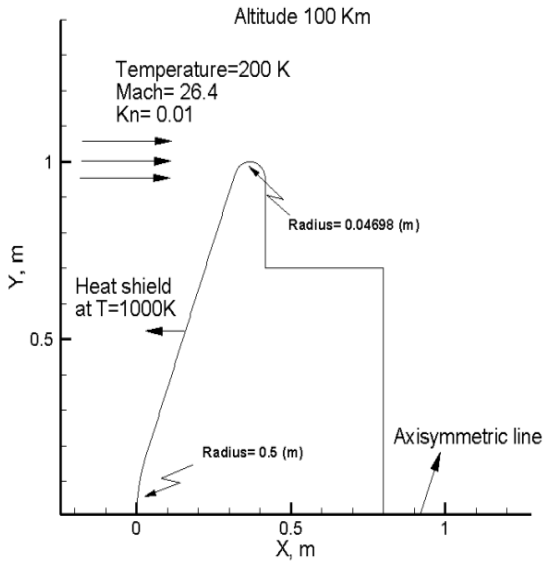

a) Schematic of the re-entry geometry

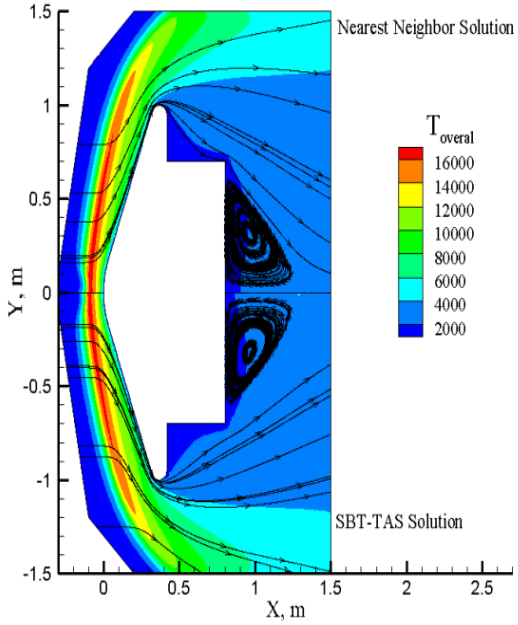

b) Temperature contours from NN and SBT-TAS

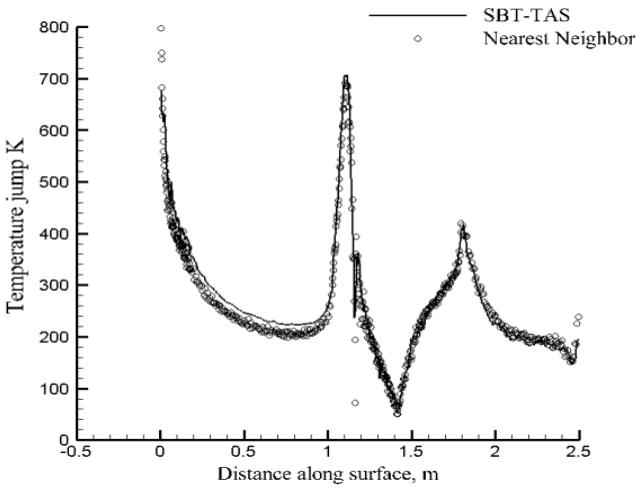

c) Temeperature jump over the geometry surface: comparison of the NN and SBT-TAS

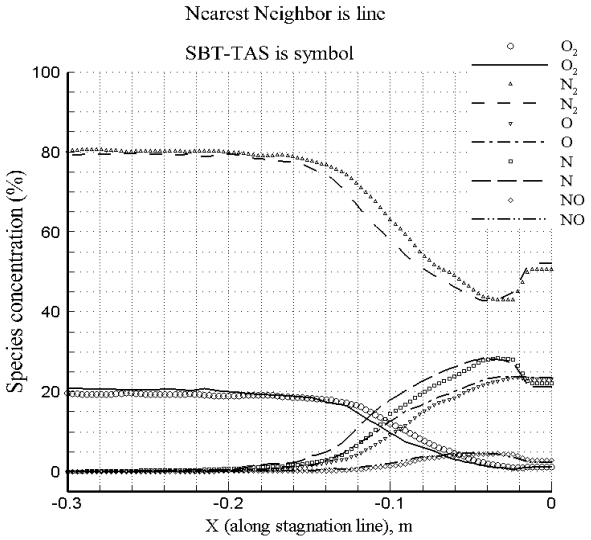

d) Species concentration: comparison of the NN and SBT-TAS

Fig. 37: Comparison of SBT-TAS and NN solutions for re-entry flow with chemical reactions [85].

5. Concluding remarks

The current paper provides a review of the DSMC collision schemes, originating either from the Boltzmann equations (i.e., TC, NTC, NN) or the Kac stochastic model (i.e., MFS, null collision, BT, SBT

families). Collision models derived from the Boltzmann equation are derived according to the principles of the classic kinetic theory, i.e., considering the concept of a collision cylinder and the maximum number of collisions that could occur in the ratio of the collision cylinder volume to the cell volume. These models needs around 10-20 particles per cell and usually suffer from eventually repeated collisions. On other side, the straightforward attempt to prevent repeated collision makes the collision frequency incorrect for small number of particle in cell. The models based on the Kac stochastic model are mainly derived from it by using mathematical operations, i.e., simplification and re-arrangement of the transition operator ($G(t)$) that appears in the Kac stochastic equation. These approximations keep the basic properties of the Kac model within small enough time step at arbitrary mean number of particles in cells when the time step and cell size are coupled in an appropriate manner. The first Kac-based models, such as the BT and Pseudo-Poisson (collision frequency) models, suffered from high computational costs, while a newly developed collision class, called the Simplified Bernoulli trial (SBT), has comparable computational costs to the standard models based on the Boltzmann equation such as NTC. A wide spectrum of rarefied flow test cases, ranging from simple equilibrium collision frequency to complicated shock-shock interactions and chemically reacting flows, was simulated by using the SBT collision family models and it was shown that SBT collision family could provide accurate solutions using small particles per cell. The benefit of the SBT collision model will be more clearly pronounced in complex 3D simulations, where a large number of particles is required if one relies on the standard NTC scheme. A hybrid NTC-SBT scheme could be also utilized for these complex 3D cases [88-89].

Acknowledgements

The first author would like to acknowledge financial supports of Ferdowsi University of Mashhad under grant No. 39035. The second author would like to acknowledge the financial support provided by the EU network program H2020 under grant MIGRATE No. 643095.

Appendix

Algorithm for sampling from the Poisson distribution:

Input: $(\delta t \times \upsilon_0)$

Output: int (n-1)

$L = e^{-\upsilon_0 t}$

a=1

n=1

while $a \geq L$

$U_n = Rand(seed)$

$a = U_n a$

$n = n + 1$

End

References

1. Karniadakis, G. E, Beskok, A., Aluru, N., Microflows and nanoflows: fundamentals and simulation, Springer Science & Business Media, 2006.
2. Mohammadzadeh, A., Roohi, E., Niazmand, H., Stefanov, S., Myong, R.S., Thermal and second-law analysis of a micro- or nano-cavity using direct-simulation Monte Carlo, Physical Review E., Vol. 85, 056305, 2012.
3. Kennard, E.H., Kinetic Theory of Gases: With an Introduction to Statistical Mechanics. McGraw-Hill, 1938.
4. Kac, M., Probability and related topics in physical sciences. Interscience Publishers Ltd., London, 1959.
5. M. Kac, *Probability and Adjacent Questions* (M., Mir, 1965) (in Russian).
6. Bird, GA. Monte Carlo simulation of gas flows. Annual Rev Fluid Mechanics 1978; 10:11–31.
7. Bird, G. A., Molecular Gas Dynamics, Oxford: Clarendon Press, 1976.
8. Bird, G. A., Molecular Gas Dynamics and the Direct Simulation of Gas Flows, Oxford: Clarendon Press, 1994.

9. Yanitskiy, V. Operator approach to Direct Simulation Monte Carlo theory in rarefied gas dynamics. In Proc. 17th Symposiums on Rarefied Gas Dynamics, A.Beylich ed. VCH, Weinheim, 770-777, 1990.
10. Ivanov, M. S., Rogasinskii, S. V., Theoretical analysis of traditional and modern schemes of the DSMC method, In Proc. 17th Symposiums on Rarefied gas dynamics, A.Beylich ed. VCH, Weinheim, 629-642, 1990.
11. Bird, G.A., Approach to translational equilibrium in a rigid sphere gas, Phys. Fluids, 6, pp. 1518-1519 1963.
12. G.A. Bird. Aspects of the Structure of Strong Shock Waves. *Phys. Fluids*, 13(5):1172, 1970.
13. Bird, G.A., The DSMC Method, CreateSpace Independent Publishing Platform, 2013.
14. Bird, G. A., The Perception of Numerical Methods in Rarefied Gas Dynamics, in Proc. 16th Int. Sym. on Rarefied Gas Dynamics, E. P. Muntz, D. Weaver and D. Campbell, eds, AIAA, Washington, DC, 1989, pp. 211.
15. Bird, G. A., Shock Wave Structure in a Rigid Sphere Gas, in Proc. 4th Int. Sym. on Rarefied Gas Dyn., J. H. de Leeuw, eds, Academic Press, New York, p. 216, 1965.
16. Koura, K., Null-collision technique in the direct-simulation Monte Carlo method. Physics of Fluids (1958-1988), 29(11), 3509-3511, 1986.
17. Nanbu, K., Direct Simulation Scheme Derived from the Boltzmann-Equation .I. Monocomponent Gases. J Phys Soc Jpn 49(5), 2042-2049, 1980.
18. Baker, L. L., Hadjiconstantinou, N. G., Variance reduction for Monte Carlo solutions of the Boltzmann equation. Physics of Fluids (1994-present), 17, 051703, 2005.
19. Homolle, T.M.M., Hadjiconstantinou, N.G., Low-variance deviational simulation Monte Carlo, Phys Fluids 19(4), 2007.
20. Homolle, T.M.M., Hadjiconstantinou, N.G., A low-variance deviational simulation Monte Carlo for the Boltzmann equation, J Comput Phys 226(2), 2341-2358, 2007.
21. Dimarco, G., Pareschi, L., Fluid solver independent hybrid methods for multiscale kinetic equations. SIAM Journal on Scientific Computing, 32, 603-634, 2010.

22. Belotserkovskii, O. M., Yanitskiy, V. E., The statistical particles-in-cells method for solving rarefied gas dynamics problems, USSR Computational Mathematics and Mathematical Physics, 15, 101-114, 1975.
23. Stefanov, S. K., Particle Monte Carlo algorithms with small number of particles in grid cells. In Numerical Methods and Applications, Springer, 110-117, 2011.
24. Stefanov, S. K., On DSMC calculations of rarefied gas flows with small number of particles in cells. SIAM Journal on Scientific Computing, 33, 677-702, 2011.
25. Goshayeshi, B., Roohi, E., Stefanov, S., A Novel Bernoulli Trials Collision Scheme in the DSMC Method with Intelligence over Particle Distances, Physics of Fluid, Vol. 27(10), 107104, 2015.
26. Gallis, M. A., Torczynski, J. R., Rader, D. J., Bird, G. A., Convergence behavior of a new DSMC algorithm. *Journal of Computational Physics*, 228(12), 4532-4548, 2009.
27. Gallis, M. A., Torczynski, J. R., Effect of collision-partner selection schemes on the accuracy and efficiency of the direct simulation Monte Carlo method, International Journal for Numerical Methods in Fluids, 67(8), 1057-1072, 2011.
28. LeBeau, G. J., Boyles, K. A., Lumpkin, F. E., Virtual sub-cells for the direct simulation Monte Carlo method, American Institute of Aeronautics and Astronautics, AIAA 2003-1031, 2003.
29. Bird, G. A., Visual DSMC Program for Two-Dimensional and Axially Symmetric Flows, The DS2V Program User's Guide, Ver. 2.1, G.A.B. Consulting Pty Ltd, Sydney, Australia, 2003.
30. Goshayeshi, B., Roohi, E., Stefanov, S., DSMC Simulation of Hypersonic Flows Using an Improved SBT-TAS Technique, Journal of Computational Physics, Vol. 303(C), pp. 28-44, 2015.
31. Khlopkov, Y. I., Zharov, V. A., Khlopkov, A. Y., Myint, Z. Y. M. Development of Monte Carlo Methods in Hypersonic Aerodynamics. *Universal Journal of Physics and Application*, *8*(4), 213-220, 2014.
32. Kogan, M. N., *Rarefied Gas Dynamics* (M., Science, 1967)
33. Lutišan, J., The Treatment of Molecular Collisions in DSMC Methods, Molecular Simulation, 14:3, 189-206, 1995.
34. von Neumann, J., Various techniques used in connection with random digits. Monte Carlo methods, Nat. Bureau Standards, 12, pp. 36–38, 1951.

35. Stefanov, S., and C. Cercignani, Monte Carlo simulation of Bénard's instability in a rarefied gas, *European journal of mechanics. B, Fluids* 11.5, pp. 543-554, 1992.
36. Bird, G. A., Sophisticated versus simple DSMC, Proceedings of the 25th International Symposium on Rarefied Gas Dynamics, St. Petersburg, Russia. 2006.
37. Bird, G.A., Sophisticated DSMC: Notes prepared for a short course at the DSMC07 meeting, Santa Fe, USA, 2007.
38. Bird, G. A., Gallis, M. A., Torczynski, J. R., Rader, D. J., Accuracy and efficiency of the sophisticated direct simulation Monte Carlo algorithm for simulating noncontinuum gas flows, Phys. Fluids 21, 017103, 2009.
39. Gallis, M.A., Torczynski, J.R., Effect of collision-partner selection schemes on the accuracy and efficiency of the direct simulation Monte Carlo method, International Journal for Numerical Methods in Fluids, 67(8), 1057-1072, 2011.
40. Macrossan, Michael N. "Searching for a near neighbor particle in DSMC cells using pseudo-subcells." *Journal of Computational Physics* 229.17 (2010): 5857-5861.
41. Meiburg, E., 1986, Comparison of the molecular dynamics method and the direct simulation technique for flows around simple geometries, Physics of Fluids, 29:3107
42. Mareschal, M., ed. Microscopic simulations of complex flows. Vol. 236., Nato ASI Series, Plenum Press, New York, 1990.
43. Bird, G.A., Direct simulation of high-vorticity gas flows, Phys. Fluids 30, 364, 1987.
44. Stefanov, S., Boyd, I. D., Cai, C.P., Monte Carlo analysis of macroscopic fluctuations in a rarefied Hypersonic flow around a cylinder, Physics of Fluids, 12, 1226-1239, 2000.
45. Stefanov, S., Roussinov, V., Cercignani, C., Rayleigh-Bénard flow of a rarefied gas and its attractors. I. Convection regime, Physics of Fluids, 14, 2255–2269, 2002.
46. Bird, G.A., Visual DSMC program for two-dimensional and axially symmetric flows, in: The DS2V Program User's Guide, Ver. 2.1, 2003.
47. Bird, G.A., The DS2V/3V program suite for DSMC calculations, in: 24th International Symposium, in: Rarefied Gas Dynamics, Vol. 762, American Institute of Physics, 2005, pp. 541–546.

48. Su, C. C., Tseng, K. C., Cave, H. M., Wu, J. S., Lian, Y. Y., Kuo, T. C., Jermy, M. C., Implementation of a transient adaptive sub-cell module for the parallel-DSMC code using unstructured grids, Computers & Fluids 39, pp. 1136-1145, 2010.
49. Amiri, A., Roohi, E., Stefanov, S., Nami, H., Niazmand, H., DSMC Simulation of Micro/Nano Flows using SBT-TAS Technique, Computers & Fluids, Vol. 102, pp. 266-276, 2014.
50. Feller, W., An Introduction to Probability Theory and its Applications, John Wiley & Sons, New York, 1971.
51. Deshpande, S. M., Subba Raju, P.V., Monte Carlo simulation for molecular gas dynamics, *Sadhana* 12.1-2 (1988), 105-123.
52. Koura, K., Transient Couette flow of rarefied binary gas mixtures, *Physics of Fluids (1958-1988)* 13.6 (1970): 1457-1466.
53. Ivanov, M.S., Rogasinsky, S.V., Rudyak, V. Y., Direct statistical simulation method and master kinetic equation. *Progr. Astro. Aero.*, 117:171-181, 1989.
54. Ivanov, M.S., Rogasinsky, S.V., Comparative analysis of algorithms of direct statistical method in rarefied gas dynamics, Zhurnal Vychislitel'noi Matematiki i Matematicheskoi Fiziki, Vol. 23, 1988, p. 1058-1070. In Russian
55. Ivanov, M., Statistical simulation of reentry capsule aerodynamics in hypersonic near-continuum flows, Rhode-Saint-Genese, Belgium, von Karman Institute for Fluid Dynamics, RTO-EN-AVT-194, 2011
56. Knuth, D.E., Seminumerical Algorithms, The Art of Computer Programming, Vol. 2, Addison Wesley, 1969.
57. Amiri, A., Roohi, E., Niazmand, H., Stefanov, S., DSMC Simulation of Low Knudsen Micro/Nano Flows using Small Number of Particles per Cells, Journal of Heat Transfer, Vol. 135, 101008, 2013.
58. Gallis, M. A., Torczynski, J. R., Rader, D.J., Molecular gas dynamics observations of Chapman-Enskog behavior and departures therefrom in nonequilibrium gases, Phys. Rev. E 69, 042201, 2004.
59. Rader, D. J., Gallis, M. A., Torczynski, J. R., Wagner, W., Direct simulation Monte Carlo convergence behavior of the hard-sphere-gas thermal conductivity for Fourier heat flow, Physics of Fluids (1994-present), 18(7), 077102, 2006.

60. Taheri, E., Roohi, E., Stefanov, S., Evaluation of the SBT collision model for near-continuum nano Fourier flows, First MIGRATE Summer School & Workshop, France, 2016.
61. John, B., Gu, X.J. and Emerson, D.R., Investigation of heat and mass transfer in a lid-driven cavity under nonequilibrium flow conditions, Numerical Heat Transfer, Part B, Vol. 58, pp. 287–303, 2010.
62. John, B., Gu, X.J. and Emerson, D.R., Effects of incomplete surface accommodation on non-equilibrium heat transfer in cavity flow: A parallel DSMC study, Computers & Fluids, Vol. 45, pp. 197–201, 2011.
63. H. Akhlaghi, E. Roohi, S. Stefanov, A New iterative wall heat flux specifying technique in DSMC for heating/cooling simulations of MEMS/NEMS, International Journal of Thermal Sciences, 59, 111-125, 2012.
64. Mohammadzadeh, A., Roohi, E., Niazmand, H., Stefanov, S., Myong, R.S., Thermal and second-law analysis of a micro- or nanocavity using direct-simulation Monte Carlo, Physical Review E, 85, 056305, 2012.
65. Mohammadzadeh, A., Roohi, E., Niazmand, H., A parallel DSMC investigation of monatomic/diatomic gas flows in micro/nano cavity, Numerical Heat Transfer, Part A: Applications, 63, 305-325, 2013.
66. Akhlaghi, H., Roohi, E., A Novel Algorithm for Implementing Specified Wall Hat Flux in DSMC: Application to Micro/Nano Flows and Hypersonic Flows, Computers and Fluids, Vol. 127, 78-101, 2016.
67. Mohammadzadeh A, Rana A, Struchtrup H. DSMC and R13 modeling of the adiabatic surface. International Journal of Thermal Sciences, Vol. 101, 9-23, 2016.
68. Shoja-Sani, A., Roohi, E., Kahrom, M., Stefanov, S., Investigation of Rarefied Gas Flow around NACA 0012 Airfoils using DSMC and NS solvers, European Journal of Mechanics, Part B: Fluids, Vol. 48, 59-74, 2014.
69. Le, N., Shoja Sani, A., Roohi, E., Rarefied gas flow simulations of NACA 0012 airfoil and sharp 25-55 biconic subject to high order nonequilibrium boundary conditions in CFD, Aerospace Science and Technology, Vol. 41, pp. 274-288, 2015.

70. Allegre, J., Raffin, M., and Lengrand, J. C., Experimental Flow fields Around NACA 0012 Airfoils Located in Subsonic and Supersonic Rarefied Air Streams, *Numerical Simulation of Compressible Navier–Stokes Flows*, edited by M. O. Bristeau, R. Glowinski, J. Periaux, and H. Viviand, Friedr.Vieweg and Sohn, Braunschweig, Germany 1985; 59–68.
71. Allegre, J., Raffin, M., and Gottesdient, L., Slip Effect on Supersonic Flow fields Around NACA 0012 Airfoils, *Rarefied Gas Dynamics 15*, edited by V. Boffi. and C. Cercigani 1986; 548–557.
72. Darbandi, M., Roohi, E., Study of Supersonic-Subsonic Gas Flows through Micro-Nano Scale Nozzles Using Unstructured DSMC Solver, Microfluidics and Nanofluidics, Vol. 10, 321-335, 2011.
73. Sebastião, I. B., Santos, W. F. Numerical simulation of heat transfer and pressure distributions in micro nozzles with surface discontinuities on the divergent contour. Computers & Fluids, 92, 125-137, 2014.
74. Sebastião, I. B., Santos, W. F. Impact of surface discontinuities on flowfield structure of a micro nozzle array. Nanoscale and Microscale Thermophysical Engineering, 18(1), 54-79, 2014.
75. Lijo, V., Setoguchi, T., Kim, H.D, Analysis of Supersonic Micro nozzle Flows, Journal of Propulsion and Power, Vol. 31(2), 754-757, 2015.
76. Saadati, A., Roohi, E., Detailed Investigation of Flow and Thermal Field in Micro/Nano Nozzle using Simplified Bernouli Trial (SBT) Collision Scheme in DSMC, Aerospace Science and Technology, Vol. 46, pp. 236-255, 2015
77. Lofthouse, A. J., Boyd, I. D., Wright, J.M., Effects of continuum breakdown on Hypersonic aerothermodynamics, Physics of Fluids, 19, 027105, 2007.
78. Su, C. C., Tseng, K. C., Wu, J. S., Cave, H. M., Jermy, M. C., Lian, Y. Y, Two-level virtual mesh refinement algorithm in a parallelized DSMC Code using unstructured grids, Computers & Fluids, 48, pp. 113–124, 2011
79. Su, C. C., Wu, J. S., Lo, M. C., Kuo, F. A., Development of parallel direct simulation Monte Carlo method using a cut-cell Cartesian grid on a single graphics processor, Computers & Fluids 101, pp. 114–125, 2014
80. Knight, D., RTO WG 10: Test Cases for CFD Validation of Hypersonic Flight, AIAA 2002-0433, American Institute of Aeronautics and Astronautics, Reston, VA, 2003.

81. Holden, M.S., Wadhams, T.P., Candler, G.V., Harvey, J.K., Measurements of Regions of Low Density Laminar Shock Wave/Boundary Layer Interactions in Hypersonic Flows and Comparison with Navier-Stokes Predictions, AIAA 2003- 1131, VA, 2003.
82. Moss, J. N., Bird, G.A., Direct simulation Monte Carlo simulations of Hypersonic flows with shock interactions, AIAA journal 43 (12), pp. 2565-2573, 2005.
83. Harvey, J. K., A review of a validation exercise on the use of the DSMC method to compute viscous/inviscid interactions in hypersonic flow, AIAA paper 3643, 2003.
84. Titov, E., Burt, J., Josyula, E., Nompelis, I., Implications of Slip Boundary Conditions on Surface Properties in Hypersonic Flows, AIAA 2012-3307**,** 43rd AIAA Thermophysics Conference, New Orleans, 2012.
85. Goshayeshi, B., Roohi, E., DSMC simulation over reactive flow of a re-entry vehicle using SBT-TAS, the first international and 3rd national conference of Iranian aerospace propulsion association, Isfahan, Iran, 22-23 October 2014.
86. Bird, G.A, Simulation of multi-dimensional and chemically reacting flows, Rarefied Gas Dynamics: Proceedings of the 11th International Symposium, edited by R. Campargue, Vol. 1, Paris, 1979, pp. 365-388.
87. Gupta, R.N., Yos J.M., Thompson R.A., A Review of Reaction Rates and Thermodynamic Transport Properties for an 11-Species Air Model for Chemical and Thermal Non Equilibrium Calculations to 30,000 K. NASA TM 101528, 1989.
88. Stefanov, S., V. Roussinov, and C. Cercignani. "Rayleigh–Bénard flow of a rarefied gas and its attractors. I. Convection regime." Physics of Fluids 14, no. 7 (2002): 2255-2269.
89. S. Stefanov, V. Roussinov, C.Cercignani, Rayleigh-Benard flow of a rarefied gas and its attractors. Part 2: Chaotic and periodic convective regimes, Physics of Fluids, 14, No 7, pp. 2270-2288 (2002) etc.